Biases in Thorpe-Scale Estimates of Turbulence Dissipation. Part I: Assessments from Large-Scale Overturns in Oceanographic Data

Citation	Mater, B. D., Venayagamoorthy, S. K., St. Laurent, L., & Moum, J. N. (2015). Biases in Thorpe-Scale Estimates of Turbulence Dissipation. Part I: Assessments from Large-Scale Overturns in Oceanographic Data. Journal of Physical Oceanography, 45(10), 2497-2521. doi:10.1175/JPO-D-14-0128.1
DOI	10.1175/JPO-D-14-0128.1
Publisher	American Meteorological Society
Version	Version of Record
Terms of Use	http://cdss.library.oregonstate.edu/sa-termsofuse

Biases in Thorpe-Scale Estimates of Turbulence Dissipation. Part I: Assessments from Large-Scale Overturns in Oceanographic Data

BENJAMIN D. MATER AND SUBHAS K. VENAYAGAMOORTHY

Department of Civil and Environmental Engineering, Colorado State University, Fort Collins, Colorado

LOUIS ST. LAURENT

Woods Hole Oceanographic Institution, Woods Hole, Massachusetts

JAMES N. MOUM

College of Earth, Ocean, and Atmospheric Sciences, Oregon State University, Corvallis, Oregon

(Manuscript received 3 July 2014, in final form 17 June 2015)

ABSTRACT

Oceanic density overturns are commonly used to parameterize the dissipation rate of turbulent kinetic energy. This method assumes a linear scaling between the Thorpe length scale L_T and the Ozmidov length scale L_O. Historic evidence supporting $L_T \sim L_O$ has been shown for relatively weak shear-driven turbulence of the thermocline; however, little support for the method exists in regions of turbulence driven by the convective collapse of topographically influenced overturns that are large by open-ocean standards. This study presents a direct comparison of L_T and L_O, using vertical profiles of temperature and microstructure shear collected in the Luzon Strait—a site characterized by topographically influenced overturns up to $O(100)$ m in scale. The comparison is also done for open-ocean sites in the Brazil basin and North Atlantic where overturns are generally smaller and due to different processes. A key result is that L_T/L_O increases with overturn size in a fashion similar to that observed in numerical studies of Kelvin–Helmholtz (K–H) instabilities for all sites but is most clear in data from the Luzon Strait. Resultant bias in parameterized dissipation is mitigated by ensemble averaging; however, a positive bias appears when instantaneous observations are depth and time integrated. For a series of profiles taken during a spring tidal period in the Luzon Strait, the integrated value is nearly an order of magnitude larger than that based on the microstructure observations. Physical arguments supporting $L_T \sim L_O$ are revisited, and conceptual regimes explaining the relationship between L_T/L_O and a nondimensional overturn size $\widetilde{L_T}$ are proposed. In a companion paper, Scotti obtains similar conclusions from energetics arguments and simulations.

1. Introduction

Vertical density overturns are commonly used to indirectly estimate the dissipation rate of turbulent kinetic energy ϵ and in turn diapycnal diffusivity in the ocean following the seminal work of Thorpe (1977) and Dillon (1982). Investigating turbulence in a thermally stratified lake, Thorpe suggested a possible correlation between an observable measure of overturn size, the so-called Thorpe length scale L_T, and a dimensionally constructed length scale previously theorized by Dougherty (1961) and Ozmidov (1965) to be a large-scale bound on isotropic motions in a stratified fluid, the so-called Ozmidov length scale $L_O \equiv (\epsilon/N^3)^{1/2}$, where $N \equiv \sqrt{-(g/\rho_0)\partial\overline{\rho}/\partial z}$ is the ambient buoyancy frequency determined from the background density gradient $\partial\overline{\rho}/\partial z$. If valid for a flow of interest, the correlation allows for inference of the microscale quantity ϵ from larger-scale motions. In an investigation of turbulence within the thermocline, Dillon (1982) provided observational evidence suggesting a linear relationship between L_T and L_O in support of Thorpe's assertion. Subsequent observations in the thermocline (Crawford 1986; Wijesekera et al. 1993; Moum 1996) and in topographically influenced turbulence (Wesson and Gregg 1994; Ferron et al. 1998) agree with

Corresponding author address: Subhas K. Venayagamoorthy, Department of Civil and Environmental Engineering, Colorado State University, 1372 Campus Delivery, Fort Collins, CO 80523. E-mail: vskaran@colostate.edu

DOI: 10.1175/JPO-D-14-0128.1

earlier findings, while indicating that the relationship is statistical in nature with a large number of samples required to realize the trend. The apparent statistical agreement shown by such studies is typically called upon in current praxis to justify use of

$$\overline{\epsilon_T} = a^2 \overline{L_T^2 N^3} \tag{1}$$

as a method for inferring the mean dissipation rate from a given set of conventionally measured density profiles, where the overbar represents some form of ensemble average. The constant of proportionality a is typically determined from an arithmetic mean (e.g., Dillon 1982) or geometric mean (e.g., Ferron et al. 1998) of L_O/L_T and is generally suggested to be close to unity. Because density profiles can be collected relatively easily and repeatedly by casts of conventional conductivity–temperature–depth devices (CTDs), Eq. (1) potentially represents an estimate of dissipation that is relatively accessible in comparison to direct measurements that require microstructure shear profilers. This practical advantage has led to a broader application of Eq. (1). A relatively recent application has been to flows in which turbulence is generated by the convective collapse of overturns that are large by open-ocean standards. In most cases, these overturns are topographically influenced and, as such, are quite distinct from the more canonical overturns of the thermocline. Because larger overturns are obvious features that evolve on observable time scales, they have been used to predict the inferred time history of the dissipation rate by applying Eq. (1) to instantaneous realizations of the density field. For example, Alford et al. (2011) employ the method to investigate the evolution of ϵ in the Luzon Strait of the South China Sea where large-amplitude internal waves and topography interact to generate overturns larger than 100 m. The method has also been employed on a time step–wise basis in a numerical subgrid routine to parameterize diapycnal mixing due to large overturning lee waves by Klymak and Legg (2010). The appropriateness of applying Eq. (1) in such flows and in such a manner is in need of verification given that early supporting work is based on ensemble averages of many samples in the relatively weak, shear-driven turbulence of the thermocline characterized by relatively small overturns (<10 m).

The goal of this paper is, therefore, to evaluate the statistical and samplewise relationship between L_T and L_O and thus the appropriateness of Eq. (1) in flows where the turbulence is predominately driven by the convective collapse of earlier stage overturns that are large compared to the turbulent motions they generate. Henceforth, we will refer to this kind of turbulence as "convectively driven"[1] in order to draw a contrast with classical "shear-driven" turbulence in which turbulence production is via homogeneous background shear (see, e.g., Rohr et al. 1988). This distinction is also made in the companion paper (Scotti 2015) that investigates this subject using direct numerical simulation (DNS). It is recognized in both papers that the two kinds of turbulence represent conceptual limits in a continuum. In the current work, we draw heavily on an analogy between the convective instabilities expected to drive turbulence in regions such as the Luzon Strait and the commonly studied Kelvin–Helmholtz (K–H) instability mechanism. Insights from the DNS work on K–H turbulence by Smyth et al. (2001) will be of particular focus. Our hypothesis is that K–H turbulence and large convective instabilities in the ocean share a common mechanism despite acting at different scales and at different Reynolds numbers. That is, both processes involve the roll up of an overturn, or "billow", that subsequently collapses into smaller-scale turbulence. Smyth et al. (2001) show the ratio L_O/L_T (L_T/L_O) to increase (decrease) monotonically with time as a K–H billow collapses. In their experiments, "young" turbulence is characterized by high available potential energy (APE) contained in large overturns, while "old" turbulence is characterized by a complex structure of smaller overturns and decreased stratification resulting from conversion of the initial APE to turbulent kinetic energy (TKE) that, in turn, increases the background potential energy through diapycnal mixing. Observations tracking billows over their life cycle in geophysical flows are rare. However, the K–H billow-following observations of Seim and Gregg (1994) loosely support the shift from $L_T > L_O$ to $L_T < L_O$ as billows evolve, with $L_T/L_O \approx 1$ on average.

In the regions of the ocean where convective instabilities are likely, we expect that the temporal dependency of L_T/L_O shown by Smyth et al. (2001) becomes increasingly relevant as the range of overturning length scales (and presumably time scales) increases. To investigate our hypothesis, the present paper focuses on three oceanic datasets from which both direct and inferred estimates of dissipation rate can be made (i.e., L_O and L_T can be independently determined). Of particular interest are observations from the Luzon Strait collected as part of the Internal Waves in Straits Experiment (IWISE). Also considered are observations from the southern Atlantic Ocean collected as part of the Brazil Basin Tracer Release Experiment (BBTRE)

[1] Our reference to convectively driven turbulence is restricted to that which follows collapse of an overturn in an otherwise stably stratified flow and not that due to a surface buoyancy flux.

where turbulence and overturning are bottom enhanced because of the rough topography as well as data collected as part of the North Atlantic Tracer Release Experiment (NATRE) where dissipation rates are more representative of the relatively quiescent ocean interior and the range of overturning scales is smaller. Details of the datasets are described in section 2. The fundamental assumptions supporting $L_T \sim L_O$ are highlighted in section 3 to set the stage for a discussion of results. Methods for calculating the relevant quantities are discussed in section 4. Results are presented in sections 5a–c that progress from global averaging of samples (section 5a), to averaging as a function of depth (section 5b), to time integration of a dissipation rates from a series of profiles (section 5c). Conclusions are presented in section 6.

2. Oceanographic datasets

The IWISE study site at the Luzon Strait is one with very strong baroclinic generation of internal tides (Simmons et al. 2011; Buijsman et al. 2014). The interaction of strong tides with steep topography along two nearly parallel north–south ridges leads to one of the most energetic internal wave environments in the World Ocean (St. Laurent et al. 2011). The acting processes range from strong shear in well-stratified mid-depth waters to hydraulically controlled turbulence in the bottommost 500 m related to lee waves (Alford et al. 2011). Data used in the current analysis were collected from a 2011 cruise deploying deep microstructure profiles at two sites over the eastern Lan-Yu Ridge and the western Heng-Chun Ridge between moorings deployed on an earlier IWISE pilot study. Over the Lan-Yu Ridge, approximately 70 profiles (58 of which are considered in the current analysis) were collected at a site along the 1000-m isobath along a crest just south of the Batan Islands. These profiles typically extend to within $O(100)$ m of the seafloor and were collected on a quasi-continuous basis (every 3–5 h) for 12 days spanning both phases of a single spring–neap tidal cycle. The Lan-Yu site, henceforth referred to as IWISE L, was characterized by both strong stratification and strong currents, apparently because of the significant influence of the Kuroshio in the upper 400 m. Outbreaks of elevated dissipation clearly occurred during instability events of the density field throughout the water column with L_T reaching $O(100)$ m in the largest cases. These overturns are extraordinary, given the highly stratified nature of the region.

Over the Heng-Chun Ridge, a total of 10 profiles (all of which are considered in the current analysis) were collected at a site along the 1800-m isobath near the center of the mooring array featured in Alford et al. (2011). This site, referred to as IWISE N2, was sampled in a quasi-continuous fashion for a single 36-h period 3–4 days after the new moon. In contrast to IWISE L, the IWISE N2 site demonstrated a relatively quiet thermocline but intense turbulence and large overturns below 1200 m, in line with the measurements of Alford et al. (2011). The dominant processes acting at IWISE N2 seem to be associated with very strong vertical velocities, suggestive of hydraulic/convective instabilities. At both IWISE sites, turbulence levels were observed to be significantly enhanced over typical oceanic levels for all phases of the tide. Further details of the cruise are contained in the technical report by St. Laurent (2012).

Turbulence at the BBTRE site ranges from rather weak internal wave-driven mixing in the thermocline waters, to stronger internal tide-driven mixing in the deep water (Polzin et al. 1997; St. Laurent et al. 2001), to hydraulically driven mixing at the bottom of fracture zone canyons (Thurnherr et al. 2005). The current study will analyze a subset of deep microstructure profiles collected in 1997 as part of the BBTRE and featured in St. Laurent et al. (2001). A total of 89 profiles extending to within $O(20)$ m of the seafloor will be considered. These profiles were taken from approximately 20° to 25°S and from 13° to 23°W and collectively integrate both spring and neap tidal periods. For the interested reader, additional details of the BBTRE survey may be found in Polzin et al. (1997) and Ledwell et al. (2000).

Unlike the IWISE and BBTRE sites, the NATRE site is one with no locally enhanced turbulent processes because of the interaction of the flow with the topography. Also unlike the IWISE and BBTRE sites, the NATRE site is favorable to double diffusion, particularly the salt-finger form of convection in the upper 1000 m (St. Laurent and Schmitt 1999). Double-diffusive convection can lead to gravitationally stable steplike temperature structures that can be easily misinterpreted as overturns (Schmitt 1994). True overturns occurring at the NATRE site are likely due to canonical internal wave activity where shear instability leads to turbulence (St. Laurent and Schmitt 1999). Thus, for turbulence properties, the NATRE site is generally representative of the open-ocean interior where the Garrett and Munk internal wave continuum is applicable and turbulent instabilities are intermittent (Munk 1981). The 136 microstructure profiles from NATRE are used here that feature data from the uppermost 2000 m. The 14 deeper profiles are also considered that extend to 3000 (10 profiles) and 4000 m (4 profiles). All profiles were collected from approximately 24° to 28°N and from 26° to 31°W and collectively integrate many tidal cycles. Additional details for the NATRE site may be found in Toole et al. (1994).

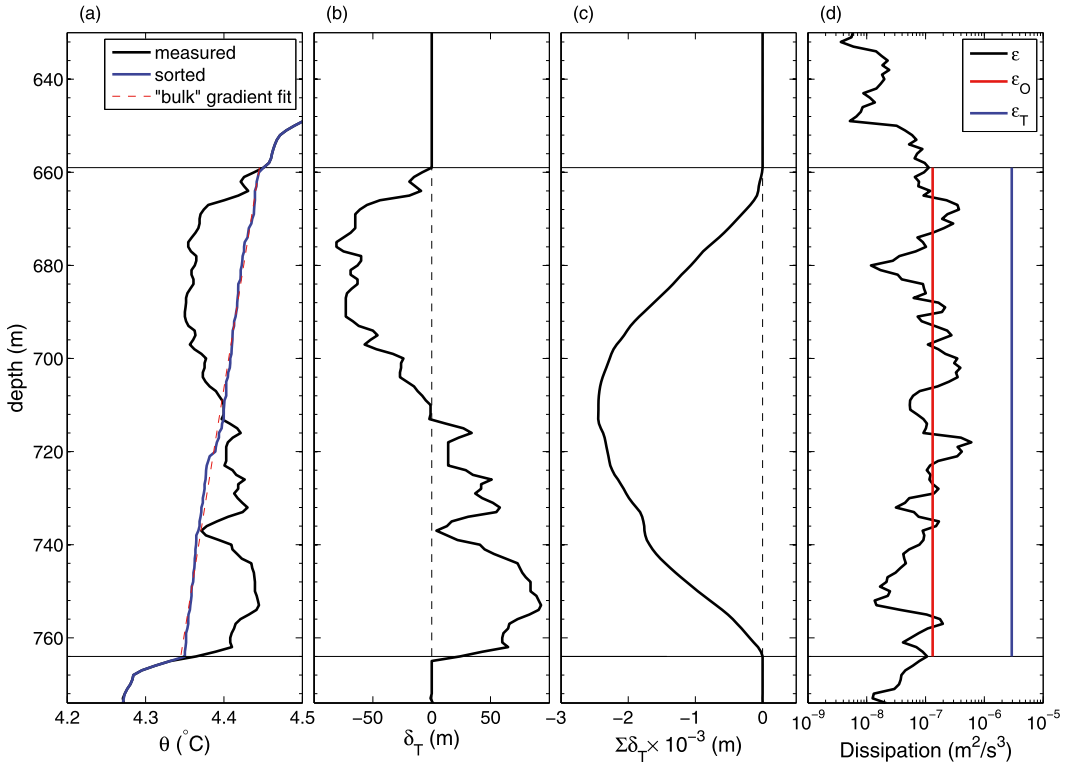

FIG. 1. Example of (a) potential temperature, (b) Thorpe displacement, (c) top-down cumulative sum of Thorpe displacements, and (d) dissipation profiles for a turbulent patch. The patch is objectively delineated using the bounds on nonzero $\sum\delta_T$.

3. Fundamentals of the Thorpe–Ozmidov relation

Fundamentally, L_T is related to the APE that is stored in a patch of turbulence at the instant of sampling. This can be shown in defining the APE (per unit mass) in terms of the Ellison length scale $L_E \equiv \langle \rho'^2 \rangle^{1/2} (\partial \overline{\rho}/\partial z)^{-1}$, such that

$$\text{APE} \equiv \frac{1}{2} N^2 L_E^2 \approx \frac{1}{2} N^2 L_T^2. \tag{2}$$

In a strict sense, the definition proposed in Eq. (2) is valid if the rms density fluctuation $\langle \rho'^2 \rangle^{1/2}$ is calculated using perturbations from the stable reference state that is obtained by three-dimensionally resorting the density field to a state of minimum potential energy as proposed by Winters et al. (1995). The reference state should also be that which defines N. In the one-dimensional limit represented by a single profile, L_T then approximates L_E, and the two length scales are equivalent if the reference density profile is linear. It is worth noting that L_T is simply a kinematic scale that describes the status of an overturn at the particular place and time of sampling and, while reflecting the APE, is not strictly defined by it. In contrast, L_O is a theoretical dynamical scale directly related to the turbulent energetics through ϵ but contains no direct information from overturns; its correlation with L_T in ocean observations is fortuitous given that L_O is derived through dimensional analysis and is typically interpreted as the scale at which inertial forces [when defined as $\rho(u_i^2/l) \sim \rho(\epsilon^2/l)^{1/3}$, where $\epsilon \sim u_i^3/l$ under the inertial subrange scaling of Taylor (1935)] balance buoyancy forces [when defined as $\rho(u_b^2/l) \sim \rho N^2 l$, with $u_b \sim Nl$] in the downscale cascade of TKE (Gregg 1987). Given the empirical nature of L_T and the theoretical nature of L_O, it is worth revisiting the fundamental conditions required for $L_T \sim L_O$.

Although theoretical support for the Thorpe–Ozmidov scaling can be cast many ways, we find the following two supporting assumptions to be most enlightening in a discussion of turbulence driven by overturn collapse: The first assumption is 1) that APE within an overturning region scales with the total turbulent kinetic energy so that $L_T \sim (\text{TKE})^{1/2} N^{-1}$. The second assumption is 2) that the overturns inertially transfer their kinetic energy downspectrum at a rate equal to ϵ so that $\text{TKE} \sim (\epsilon L_T)^{2/3}$; that is, overturns are associated with isotropic motions of the inertial subrange under Kolmogorov's second similarity hypothesis. If both assumptions are met, it follows that

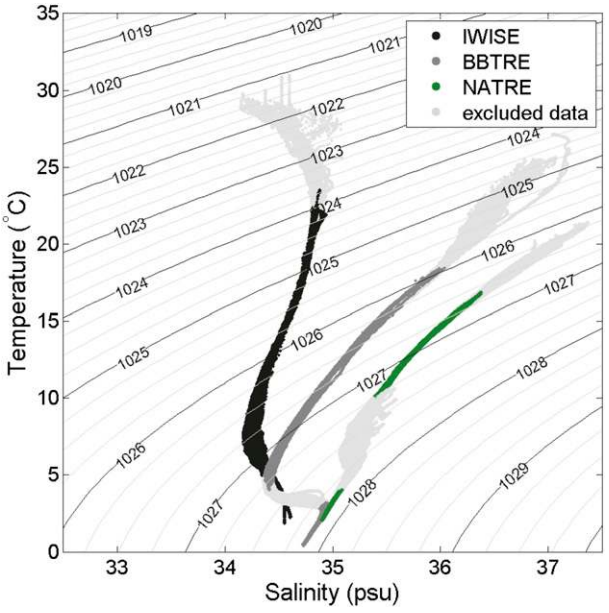

FIG. 2. *T–S* diagram for IWISE, BBTRE, and NATRE data. Data omitted from the analysis are shown in light gray. Density contours are kg m^{-3}.

$$\frac{1}{2}N^2L_T^2 \sim (\epsilon L_T)^{2/3} \Rightarrow L_T \sim L_O. \tag{3}$$

In other words, the turbulent Froude number defined by $\mathrm{Fr}_k \equiv \epsilon/(kN)$ is assumed to be $O(1)$ (Mater et al. 2013).

First, consider the assumptions 1 and 2 in the case of shear-driven turbulence where the APE is sourced directly from the TKE reservoir of the turbulent motions. That is, in the limit where the overturns are a product of the turbulence. In an investigation of homogeneous shear-driven turbulence of classic laboratory and DNS experiments, Mater and Venayagamoorthy (2014) show that assumption 1 is valid in a buoyancy-dominated regime for which the gradient Richardson number $\mathrm{Ri} \equiv N^2/S^2$ is equal to or greater than some critical value $\mathrm{Ri}_c \approx 0.25$ and $\mathrm{Fr}_k^{-1} > O(1)$ (see their Fig. 4), where $S = d\overline{u}/dz$ is the mean shear in the unidirectional flows studied. Evidence from Moum (1996) is suggestive that assumption 1 is similarly valid for strongly stratified shear-driven overturning in the ocean thermocline (assuming w'^2 is a loose surrogate for TKE; see his Fig. 3b). In the weakly stratified limit, however, assumption 1 fails as APE vanishes. In this well-mixed regime, overturns are relieved of the anisotropic influence of stratification—a condition more supportive of assumption 2, as suggested by the results of Mater et al. (2013) and Mater and Venayagamoorthy (2014) in what is essentially a shear-free inertia-dominated (quasi isotropic) regime. The array of classic datasets lends support to both assumptions only at the threshold between buoyancy- and inertia-dominated regimes when $\mathrm{Ri} \approx \mathrm{Ri}_c$ and $\mathrm{Fr}_k^{-1} \approx O(1)$. Dependence of L_T/L_O on the Richardson number is clearly demonstrated by Rohr et al. (1988), who explicitly show L_T/L_O to be an increasing function of Ri, with $L_T < L_O$ in the weakly stratified limit ($\mathrm{Ri} \lesssim \mathrm{Ri}_c$) and $L_T \gtrsim L_O$ when stratification is strong ($\mathrm{Ri} \gtrsim \mathrm{Ri}_c$). In light of these experimental findings, the central tendency of thermocline observations for $L_T \approx L_O$ implies consistency in Ri—an implication in line with recent observations of shear-driven turbulence in the equatorial undercurrent by Smyth and Moum (2013), who refer to this condition as "marginal instability." Therefore, it may be reasonable to expect that, on average, both assumptions hold and that Eq. (1) is valid for flows characterized by marginal instability.

Next, consider the case of convectively driven turbulence where TKE is being sourced from a larger reservoir of APE. That is, in the limit where the turbulence is a product of the overturns. It is clearly doubtful that either assumption would hold for the early stages of convectively driven turbulence when APE > TKE (see Scotti 2015) and an inertial subrange has yet to develop. Breakdown in the assumptions is an explanation for $L_T > L_O$ in the young K–H turbulence of Smyth et al. (2001). In old turbulence, adherence to the assumptions likely depends on how well the event has locally mixed the fluid. Well-mixed conditions would tend to support assumption 2, while less thorough mixing would support assumption 1. Smyth et al. (2001) find $L_T < L_O$ in support of well-mixed conditions for the old turbulence in their simulations. Unfortunately, their study did not explicitly indicate whether time averaging would result in $L_T \approx L_O$ for their class of convective instability.

4. Methods

In the current study, we consider hydrographic and turbulence measurements collected concurrently from a single platform so that temporal or spatial mismatches in overturn characteristics can be avoided. For all datasets, the platform consisted of some form of free-falling vertical microstructure profiler (VMP). Instrumentation aboard the VMPs provides direct estimates of ϵ and corresponding measurements of conductivity and temperature for the calculation of density profiles. Vertical resolution of the data considered here provides a minimum reliable Thorpe scale of $L_{T,\min} \approx 1$ m.

a. Thorpe-scale calculations for turbulent patches

The process proposed by Thorpe (1977) for determining L_T involves resorting an instantaneously observed vertical profile of potential density σ, such that the profile is monotonically increasing with depth (i.e., gravitationally stable). This is done while keeping track

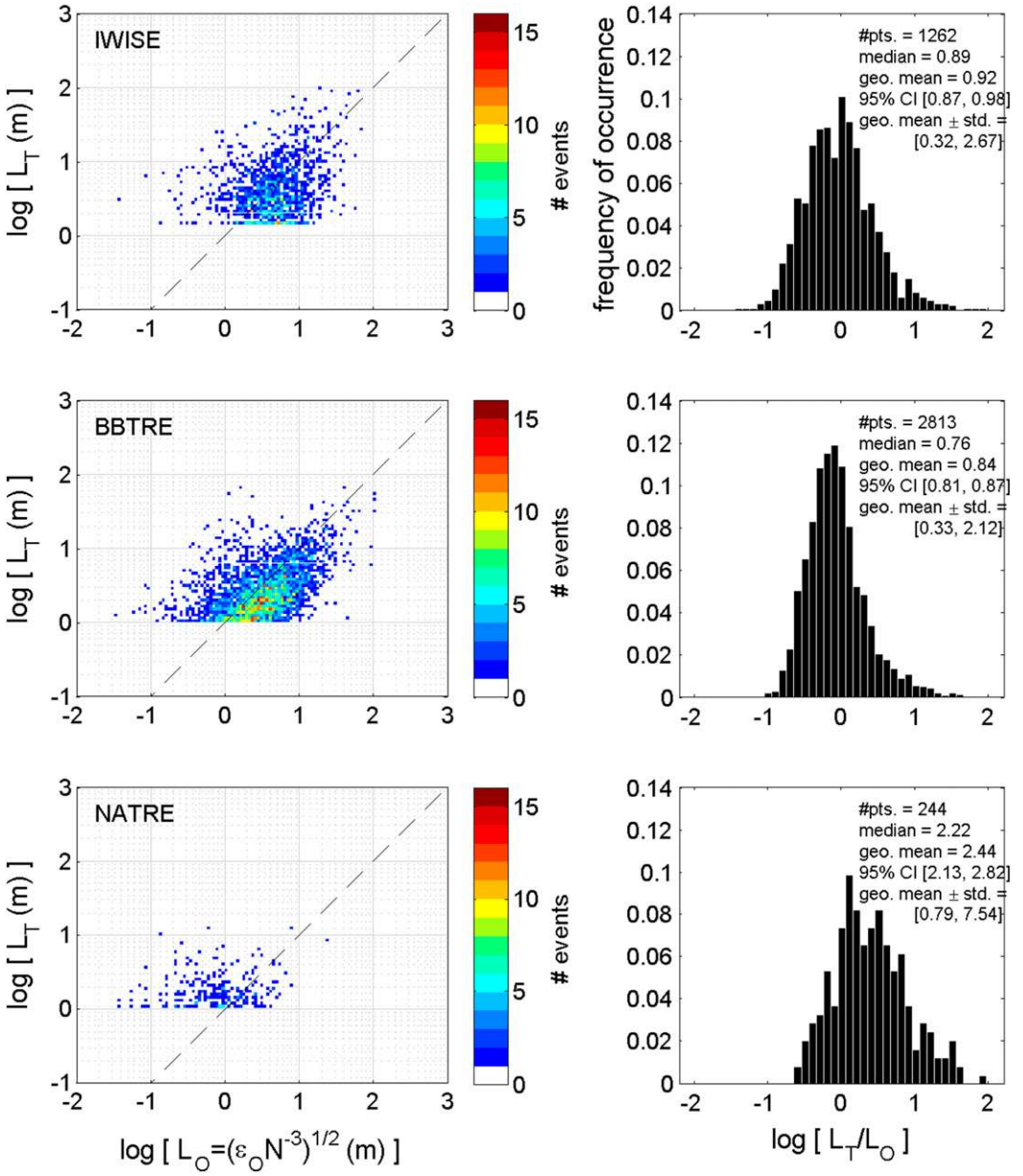

FIG. 3. Scatterplot comparisons of the Thorpe L_T and Ozmidov L_O scales calculated from turbulent patches for (top) IWISE, (middle) BBTRE, and (bottom) NATRE. Point density is represented by color bars and the 1 to 1 line is dashed. Histograms represent logarithmic ratios of ordinate to abscissa, together with measures of central tendency.

of the displacement required of each data point. For a given depth z_j, this displacement is calculated as $\delta_{Tj} = z_j - z_{\text{sorted}}$, where z_{sorted} is the depth to which the sample taken at z_j must be moved to achieve a stable profile. In this sense δ_T reflects the displacements needed of samples in the unsorted profile. For an individual overturn in quiescent fluid, δ_T is large and negative at the upper boundary, increases with depth, and is large and positive at the lower boundary so that a ''reverse Z'' signature appears in the profile of δ_T (assuming z_j is positive and increases with depth). The root-mean-square of δ_T for the depth range exhibiting this signature then determines L_T of the overturn:

$$L_T = \langle (\delta_T)^2 \rangle^{1/2}. \tag{4}$$

Because overturns are observed at various stages of development, and thus coherency, the reverse Z pattern

TABLE 1. Patchwise statistics for $a(=L_O/L_T)$ in Eq. (1). The geometric mean and standard deviations are denoted as $\langle\,\rangle_g$ and $s_g(\,)$, respectively. Values are shown for interest; all calculations use $a = 1$ except where noted.

Dataset	Median	$\langle a\rangle_g$	95% CI $\langle a\rangle_g$	$\langle a\rangle_g \pm s_g(a)$
IWISE	1.12	1.09	[1.02, 1.15]	[0.37, 3.14]
BBTRE	1.31	1.19	[1.15, 1.23]	[0.47, 3.01]
NATRE	0.45	0.41	[0.34, 0.47]	[0.13, 1.27]
Ferron et al. (1998)	—	0.90	—	[0.5, 1.8]

is not always easy to distinguish. As such, we objectively identify ''turbulent patches'' for Thorpe-scale calculations as vertical segments of the profile over which nonzero values of δ_T cumulatively sum to zero. Patch boundaries are determined using a top-down cumulative sum $\sum_{j=1}^{n}\delta_{Tj}$, where $j = 1$ corresponds to a beginning value at the top of the profile and $j = n$ corresponds to the end value at the bottom of the profile. For most of the water column, the density profile is stable so that $\sum\delta_T = 0$ because $\delta_T = 0$. Over an overturning patch, however, $\sum\delta_T$ decreases from zero as a function of depth in the uplifted heavy fluid before increasing back to zero as a function of depth in the downwelled light fluid. The depths where $\sum\delta_T = 0$ on either side of the overturning fluid delineate the patch. It is over these delineated vertical segments that patch averages of buoyancy frequency and dissipation rate are taken for a calculation of L_O. The process of identifying a turbulent patch is shown in Fig. 1, where potential temperature θ has been used as a surrogate for potential density.

b. Temperature–salinity relationships

Because of concern over the reliability of salinity measurements, we use potential temperature θ as a surrogate for potential density in determining Thorpe scales. This was done for two primary reasons: First, the conductivity cell on the VMP used at the IWISE site was unpumped and, therefore, provided estimates of salinity that were unreliable for estimating potential density at the accuracy level needed for determining L_T. Second, problems associated with determination of salinity from conductivity, temperature, and pressure can propagate into estimates of density, resulting in σ profiles with higher random and systematic noise levels than profiles of potential temperature θ (Gargett and Garner 2008). This issue is a concern for all three datasets and is especially problematic in the relatively weak stratification of near-bottom water at the BBTRE site. An obvious disadvantage of our method is the potential for wrongly counting salinity-compensated temperature inversions as density overturns. To confront this source of error, the temperature–salinity (T–S) relationships for the datasets were examined so that depths for which density was strongly a function of salinity could be omitted. Examination of T–S relationships also allowed for omission of depths characterized by considerable spread along lines of constant σ—a condition typically referred to as ''spice'' that is indicative of possible double-diffusive, nonturbulent salt fingering rather than turbulent mixing (Schmitt 1994, 1999; St. Laurent and Schmitt 1999). Figure 2 shows the T–S relationships for the data considered here. Data omitted from the current analysis are shaded in light gray. Omitted data include measurements from approximately $1027.25 \lesssim \sigma \lesssim 1027.75\,\mathrm{kg\,m^{-3}}$ in both BBTRE and NATRE that correspond to water from approximately 750–2000 m in BBTRE and from 600–2000 m in NATRE. Also excluded were data from the uppermost 200 m in IWISE and BBTRE and the uppermost 300 m NATRE that are susceptible to atmospheric influences leading to spice. For IWISE, salinity values were derived indirectly using the temperature measurements of the VMP and a fit to the T–S relationship provided by nearby and quasi-simultaneous CTD casts. It is also worth noting that our delineation of poorly behaved depth horizons is somewhat subjectively applied by visual inspection using the aggregate T–S data for a given dataset. As such, it is possible that some temperature inversions considered in the following analysis are compensated partially or fully by salinity. This issue is discussed further in appendix A wherein the method is shown to be robust enough for the purposes of this analysis. Instrument noise in the potential temperature measurements was filtered using the smoothing algorithm of Gargett and Garner (2008) with threshold values of 0.001°C for IWISE and 0.0005°C for BBTRE and NATRE.

c. Calculation of buoyancy frequency

In accordance with the discussion in section 3, the buoyancy frequency N should be that which characterizes the background stratification against that which a particular overturn is working; that is, the density profile used to calculate $\partial\overline{\rho}/\partial z$ (or more strictly $\partial\overline{\sigma}/\partial z$) should characterize the background potential energy so that perturbations from $\overline{\rho}(z)$ [or $\overline{\sigma}(z)$] characterize the potential energy available for conversion to turbulence. Unfortunately, the limitations of field sampling and the nonstationary, inhomogeneous nature of natural flows make determination of a background N nontrivial, if not impossible. Most commonly, the Thorpe-sorted density profile is used as a surrogate for that of the background state, and the gradient of the profile across a turbulent patch is calculated in some fashion. In the current work, a ''bulk'' density gradient is calculated from the

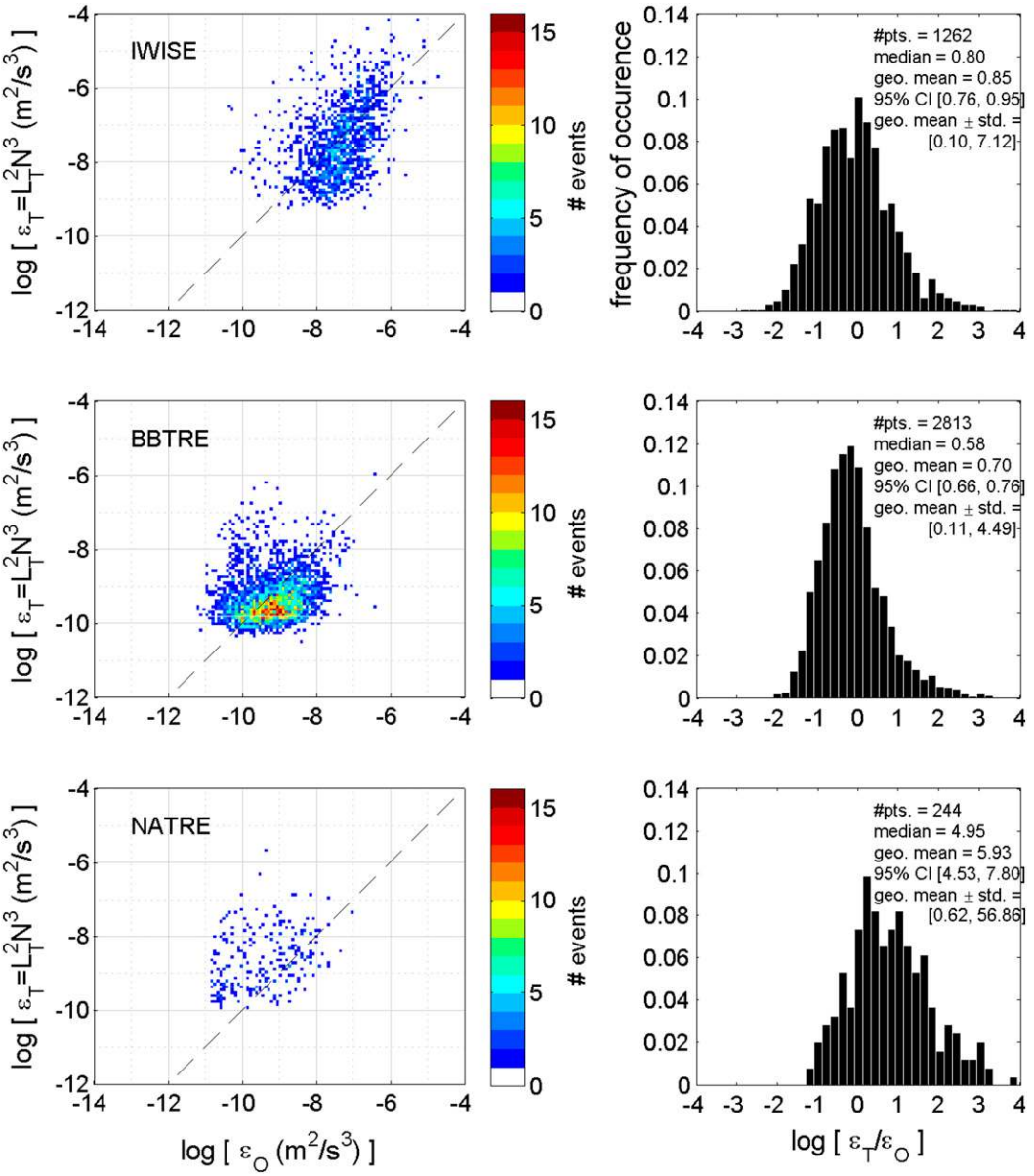

FIG. 4. Scatterplot comparison of the Thorpe scale–inferred dissipation ϵ_T and the patch-averaged measured dissipation ϵ_O.

Thorpe-sorted profile using the method of Smyth et al. (2001), wherein the approximate equivalence of the Thorpe and Ellison scales is exploited to yield

$$\left(\frac{\partial\overline{\sigma}}{\partial z}\right)_{\text{bulk}} \equiv \frac{\langle\sigma'^2\rangle^{1/2}}{L_T}. \tag{5}$$

The density perturbation σ' is determined as the difference between the instantaneous and sorted values at a given depth, the square of which is averaged over the vertical extent of the event (see Fig. 1). Since we use potential temperature as a surrogate for potential density, a ''pseudo'' potential density profile $\tilde{\sigma}(z)$ is used to determine σ'. The pseudo profile $\tilde{\sigma}$ is computed directly from the temperature profile using a constant arbitrary salinity and an approximation to the nonlinear equation of state (see Gill 1982) and, as such, provides values of the temperature-sorted equivalent density gradient needed for N but not true values of density.

Equation (5) is used in the current study because the method is relatively insensitive to the delineation of patch boundaries and, therefore, provides an appropriate estimate of N when a turbulent patch contains more than one

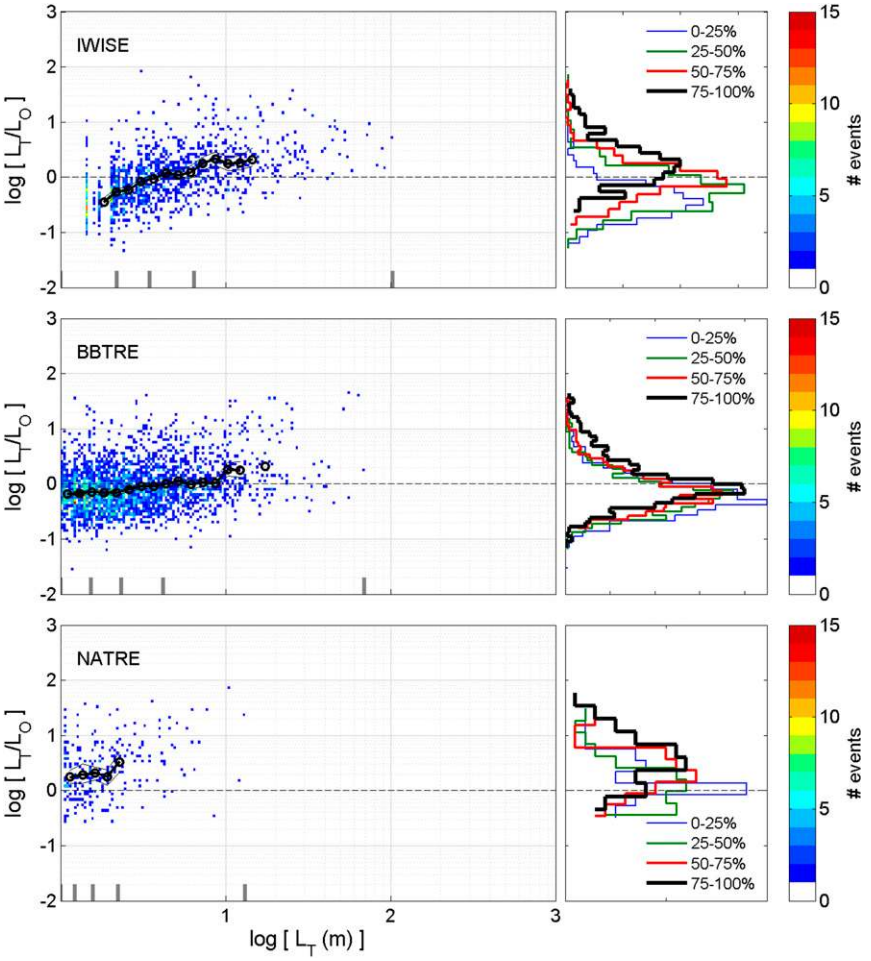

FIG. 5. Comparison of L_T/L_O with L_T, for (top) IWISE, (middle) BBTRE, and (bottom) NATRE. (left) The running mean of $\log(L_T/L_O)$ and bootstrapped 95% confidence intervals are shown for bins in $\log(L_T)$ (center points marked with circles). Only bins with more than 20 patches are considered in the calculation of the running mean. (right) Quartile distributions of the data are shown. Quartile delineations are shown with gray ticks in the left panels.

overturn (Smyth et al. 2001). Given the novelty of the method, a comparison with more common methods is provided in appendix B.

d. *Patch estimates of dissipation and Ozmidov length scale*

To allow a straightforward comparison between datasets, we assume $a = 1$ in calculating the inferred dissipation rate ϵ_T from Eq. (1). The actual value of a (in a statistical sense) for each dataset is given separately in section 5a. The dissipation rate used in calculation of L_O for a given patch is an arithmetic mean of the VMP measurements over the vertical extent of the patch (see Fig. 1). This patch-averaged dissipation will be denoted as ϵ_O, while the unaveraged VMP measurements will simply be denoted as ϵ.

5. Results

a. *Patchwise comparisons*

First, consider the direct comparison of L_T and L_O and the distribution of L_T/L_O for all turbulent patches (Fig. 3). As in Wesson and Gregg (1994), we find the data cluster near $L_T \approx L_O$ but with considerably more scatter than reported by Dillon (1982). Nonetheless, we find that L_T/L_O is lognormally distributed for all three datasets with a geometric mean that is $O(1)$. This lognormal behavior is also reported by Wijesekera et al. (1993) and Stansfield et al. (2001). The positive skewness in the NATRE data is possibly due to salinity-compensated temperature inversions resulting from the double-diffusive processes known to occur there. The bias persists in NATRE despite our elimination of depths characterized

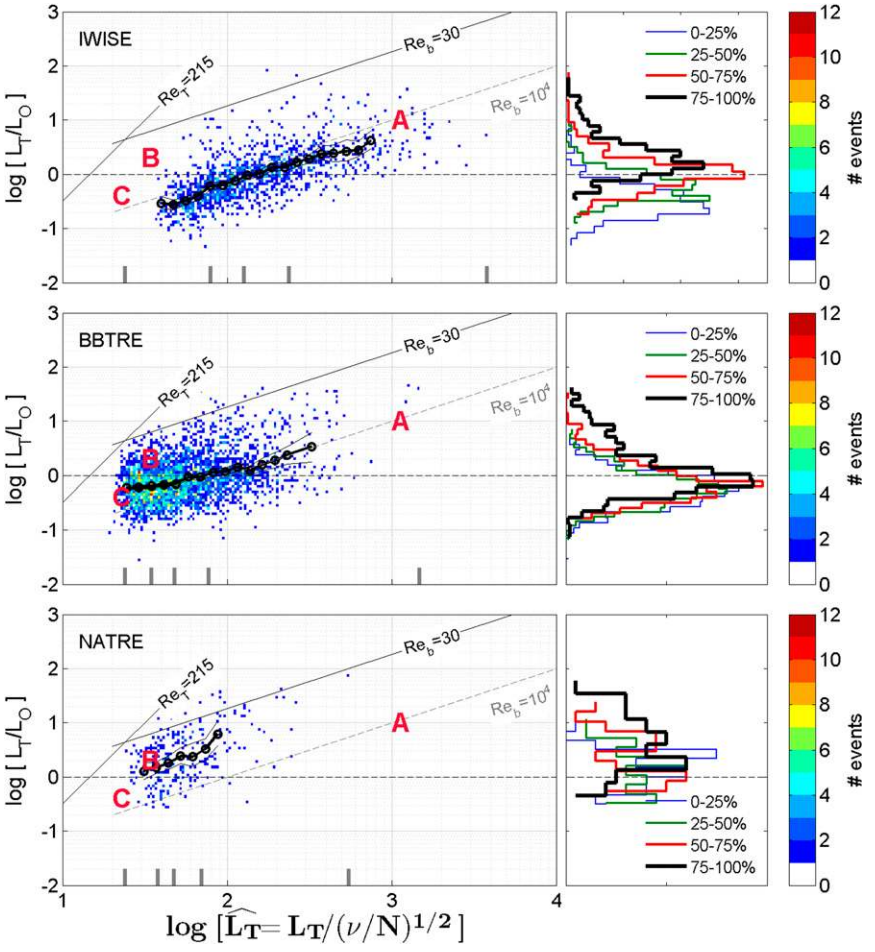

FIG. 6. Comparison of L_T/L_O with the nondimensional Thorpe scale $\widehat{L_T} = L_T/L_{\nu N}$. Conceptual regimes are labeled A (strongly forced, presumably young turbulence, and large overturns), B (weakly forced, strongly stratified turbulence, and small overturns), and C (weakly forced, weakly stratified turbulence, and small overturns; old convectively driven turbulence). (left) The running mean of $\log(L_T/L_O)$ and bootstrapped 95% confidence intervals are shown for bins in $\log(\widehat{L_T})$ (center points marked with circles). Only bins with more than 20 patches are considered in the calculation of the running mean. (right) Quartile distributions of the data are shown. Quartile delineations are shown with gray ticks in the left panels.

by obvious spice in the T–S relationship—a finding that highlights an important consideration for sorting temperature alone when turbulence is weak. Statistics of the L_T/L_O distributions for each dataset are reported in respective figures, while estimates of the coefficient a are shown in Table 1. We find that, with the exception of NATRE, the statistics compare well across datasets and that the statistical range in a is comparable to that found by Ferron et al. (1998). Statistical variability of Eq. (1) is explicitly shown in Fig. 4 and compares inferred and microstructure dissipation estimates. The distribution in ϵ_T/ϵ_O demonstrates greater spread around the geometric mean than the distribution of L_T/L_O mostly because estimates of ϵ_T involve squared values of L_T. Nonetheless, the distributions shown here suggest that use of Eq. (1) in a geometrically averaged sense is appropriate despite the presence of convectively generated turbulence. The particular application should, however, consider the spread and lognormal behavior of the data.

In the current work, we have hypothesized that L_T/L_O is dependent on the age of the convectively generated turbulence in a fashion similar to K–H billows. We therefore plot the ratio against L_T in Fig. 5 under the expectation that L_T diminishes as turbulence ages. Indeed, in apparent agreement with K–H turbulence (cf. Smyth et al. 2001), L_T/L_O and L_T demonstrate a positive correlation spanning $L_T/L_O \approx 1$ that is most obvious in

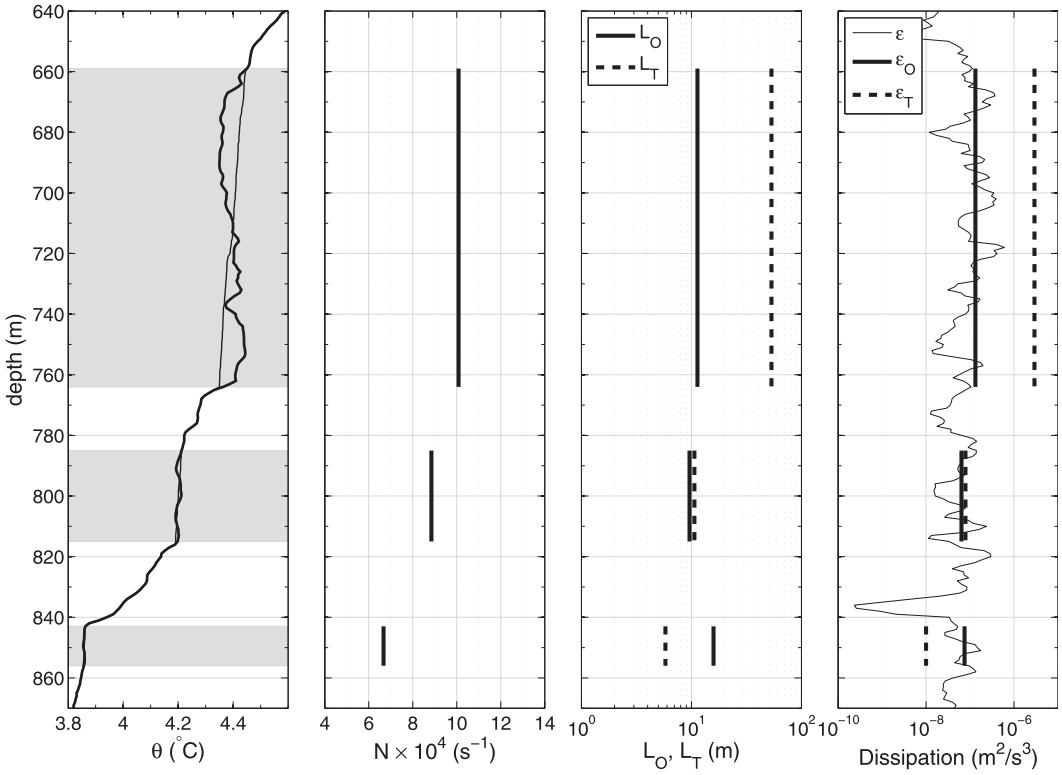

FIG. 7. Example turbulent patches from IWISE. The patch centered at 710 m falls near regime A ($\widehat{L_T} = 1760$ and $L_T/L_O = 5$) and demonstrates a large coherent overturn in relatively strong stratification, thus suggestive of a youthful overturn. The smaller patch near 800 m demonstrates $L_O \approx L_T$ and is suggestive of a transitional state between young and old turbulence ($\widehat{L_T} = 341$ and $L_T/L_O = 1.2$). The smallest patch falls near regime B ($\widehat{L_T} = 158$ and $L_T/L_O = 0.4$) and is associated with relatively weak stratification, thus suggesting old, well-mixed turbulence.

the IWISE data that perhaps best represents convectively generated turbulence. The geometric mean of L_T/L_O increases nearly monotonically with L_T for both IWISE and BBTRE, while the trend in NATRE is less convincing because of the scarcity of overturns and the bias toward large L_T/L_O potentially caused by the double-diffusive effects discussed previously. Bootstrapped 95% confidence intervals around the means for IWISE and BBTRE indicate that the trends are statistically significant. Distributions of L_T/L_O are shown as histograms in the right panels of Fig. 5 for quartiles of the data delineated by L_T. Two-sample Kolmogorov–Smirnov (K–S) testing indicates that no two quartile distributions are statistically the same for the IWISE data at the $\alpha = 5\%$ level (i.e., the observed differences in the quartile distributions have a less than 5% chance of occurring if it is assumed that the quartiles come from the same population). K–S testing of BBTRE and NATRE data indicates that only the first and second quartiles are statistically indistinguishable.

The ratio L_T/L_O also increases as a function of the nondimensional Thorpe scale $\widehat{L_T} \equiv L_T/L_{\nu N}$ (Fig. 6), where $L_{\nu N} \equiv (\nu/N)^{1/2}$ is a dimensionally constructed small scale that is independent of the turbulence and physically represents the length scale over which the viscous diffusion of momentum occurs on time scale N^{-1}. Given constant viscosity ν, $\widehat{L_T}$ expresses the size of an overturn with respect to the background stratification and, as such, $\widehat{L_T}^2$ is a nondimensional representation of APE [i.e., $\widehat{L_T}^2 = (N^2 L_T^2)/(\nu N) \sim \text{APE}/(\nu N)$, where νN is the potential energy of the smallest density fluctuations]. Therefore, $\widehat{L_T}$ allows for a conceptual and practical distinction between young overturns that have yet to mix the fluid (i.e., high APE, large $\widehat{L_T}$) from those occurring in older turbulence where significant mixing has already occurred (i.e., low APE, small $\widehat{L_T}$). That is, $\widehat{L_T}$ is conceptually a surrogate for the (inverse) age of the turbulence that is more informative than L_T. Under this reasoning, all three datasets suggest L_T/L_O should decrease with the event age as in K–H turbulence. As in Fig. 5, quartile delineations are indicated in the left panels of Fig. 6, with each quartile in IWISE, the upper three quartiles in BBTRE, and the upper two quartiles in NATRE being statistically different as indicated by two-sample K–S testing at the $\alpha = 5\%$ level. The first quartile starts at $\widehat{L_T} = 24$ to avoid resolution errors that will be discussed later.

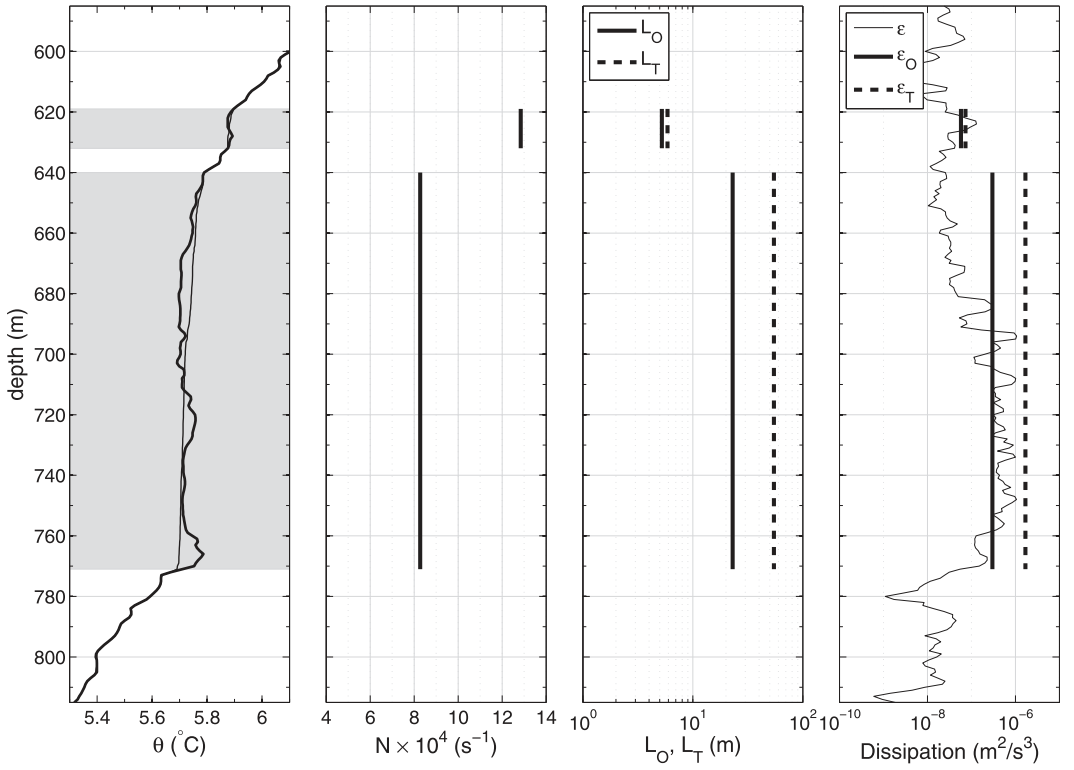

FIG. 8. Example turbulent patches from IWISE. The patch centered at 700 m falls within regime A ($\widehat{L_T} = 1654$ and $L_T/L_O = 2.6$) and demonstrates a large overturn suggestive of a youthful billow. The smaller overturn centered near 625 m is of similar size to the smallest overturn in Fig. 7 but is occurring in stronger stratification and with slightly less dissipation so that $L_T \approx L_O$. We interpret this to be representative of a transitional state between young and old turbulence ($\widehat{L_T} = 214$ and $L_T/L_O = 1.2$).

Plotting L_T/L_O against $\widehat{L_T}$ in Fig. 6 allows for a discussion various physical regimes. First note that

$$\frac{L_T}{L_O} = \mathrm{Re}_b^{-1/2}\widehat{L_T}, \tag{6}$$

so that lines of constant buoyancy Reynolds number $\mathrm{Re}_b \equiv \epsilon/(\nu N^2)$ may be constructed through the space. Following the suggestion of Gibson (1980), a line corresponding to $\mathrm{Re}_b = 30$ is drawn to approximately delineate "active" turbulence ($\mathrm{Re}_b > 30$; below line) from "fossil" turbulence ($\mathrm{Re}_b < 30$; above line). A number of patches observed in NATRE fall into the fossil regime, thus supporting the earlier suggestion that these data are representative of nonturbulent salt fingering rather than true overturning. Furthermore, Eq. (6) shows that differences in the mean trends are related to differences in Re_b between the study sites; strongly turbulent IWISE data cluster along $\mathrm{Re}_b \sim O(10^4)$, while weakly turbulent NATRE data cluster closer to the fossil-active transition. BBTRE, which features weak dissipation rates high in the water column and strong dissipation rates near bottom topography, spans a wider range in Re_b and overlaps with both NATRE and IWISE data. The apparent consistency of Re_b for a given dataset suggests that this parameter is not particularly useful in describing L_T/L_O.

Next, note that

$$\frac{L_T}{L_O} = \mathrm{Re}_T^{-3/2}\widehat{L_T}^3, \tag{7}$$

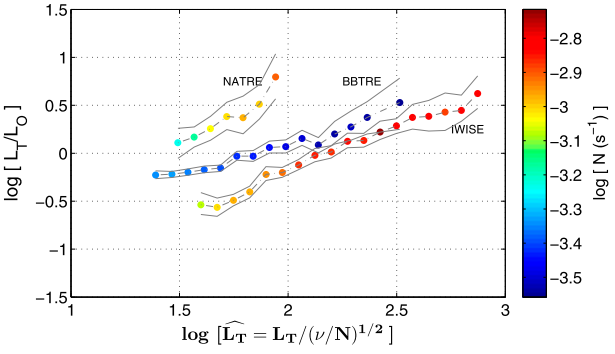

FIG. 9. Summary of the mean of $\log(L_T/L_O)$ with the nondimensional Thorpe scale $\widehat{L_T} = L_T/L_{\nu N}$. Data points and confidence intervals are the same as in Fig. 6. Mean stratification is indicated in the color bar.

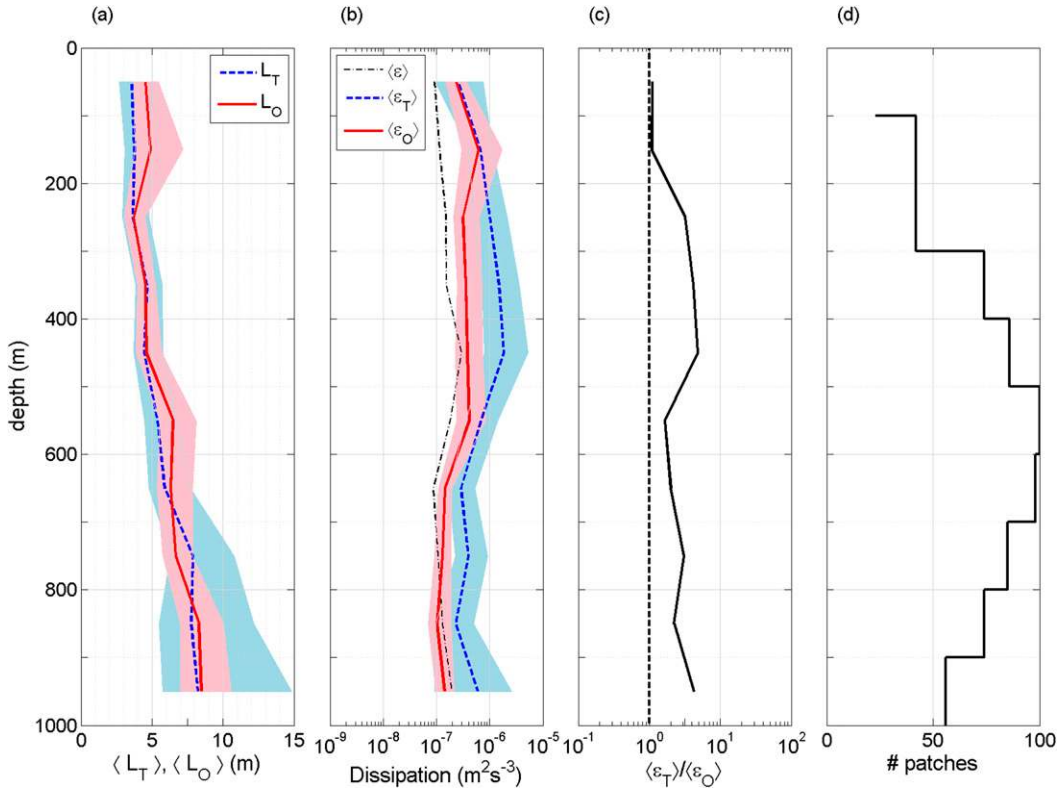

FIG. 10. Mean values as a function of depth at IWISE L during the spring tidal cycle. The 95% confidence intervals around the means are shown in the left two panels.

where $\mathrm{Re}_T \equiv (L_T/\eta)^{4/3}$ is the Reynolds number of the overturns presented by Luketina and Imberger (1989), and $\eta \equiv (\nu^3/\epsilon)^{1/4}$ is the Kolmogorov length scale. Since the minimum resolved L_T value is approximately 1 m and the approximate shear probe noise level is $O(10^{-11})\,\mathrm{m^2\,s^{-3}}$, we cannot hope to resolve turbulence with $\mathrm{Re}_T \lesssim 215$. Using this value, Eq. (7) is plotted in Fig. 6 to indicate where the data have been truncated because of these restrictions. There may well be some weakly turbulent overturns above this line that are not resolved. In recognition of this truncation, the quartile distributions do not consider data with $\widehat{L_T} < 24$ that results from Eqs. (6) and (7) given $\mathrm{Re}_{b,\min} = 30$ and $\mathrm{Re}_{T,\min} = 215$; only for $\widehat{L_T} \gtrsim 24$ is L_T/L_O limited physically by the stratification rather than artificially by measurement resolution.

Now consider the three regimes loosely labeled A–C in Fig. 6. The labels are positioned to aid in a qualitative discussion of data and are not intended to quantitatively delineate regimes. In regime A, forcing is strong with respect to the background stratification (large $\widehat{L_T}$), and $L_T > L_O$ suggests the stratification is strong with respect to the turbulence. This regime is populated by large, presumably young overturns of the IWISE and BBTRE datasets. The convective nature of the IWISE overturns suggests $L_T > L_O$ in regime A is likely because APE > TKE, that is, a violation of assumption 1. Assumption 2 is also expected to be violated because the turbulence is, presumably, not yet fully developed and is strongly anisotropic at the outer scales. The largest patches shown in Figs. 7 and 8 are exemplary of IWISE events from regime A. The largest patch in Fig. 7 demonstrates a L_T value that is 5 times larger than L_O as well as a coherent overturn shape and strong stratification. These characteristics are suggestive of young turbulence. The large patch in Fig. 8 may also represent young turbulence, albeit slightly more developed than the large patch of Fig. 7 as indicated by the decreased coherency of the overturn shape, the closer agreement between L_T and L_O ($L_T/L_O = 2.6$), and the weaker stratification.

IWISE and BBTRE data extend from regime A into regime C where overturns are presumably due to older, developed turbulence that has mixed the flow and reduced the stratification such that $L_T < L_O$. Regime C likely corresponds with either the shear-dominated or inertia-dominated (quasi isotropic) regimes of Mater and Venayagamoorthy (2014) discussed in section 3. The discussion in section 3 suggests possible adherence to assumption 2 in regime C but a breakdown in assumption 1 as stratification becomes weak. The overturns in Fig. 7 represent the transition from A to C, with

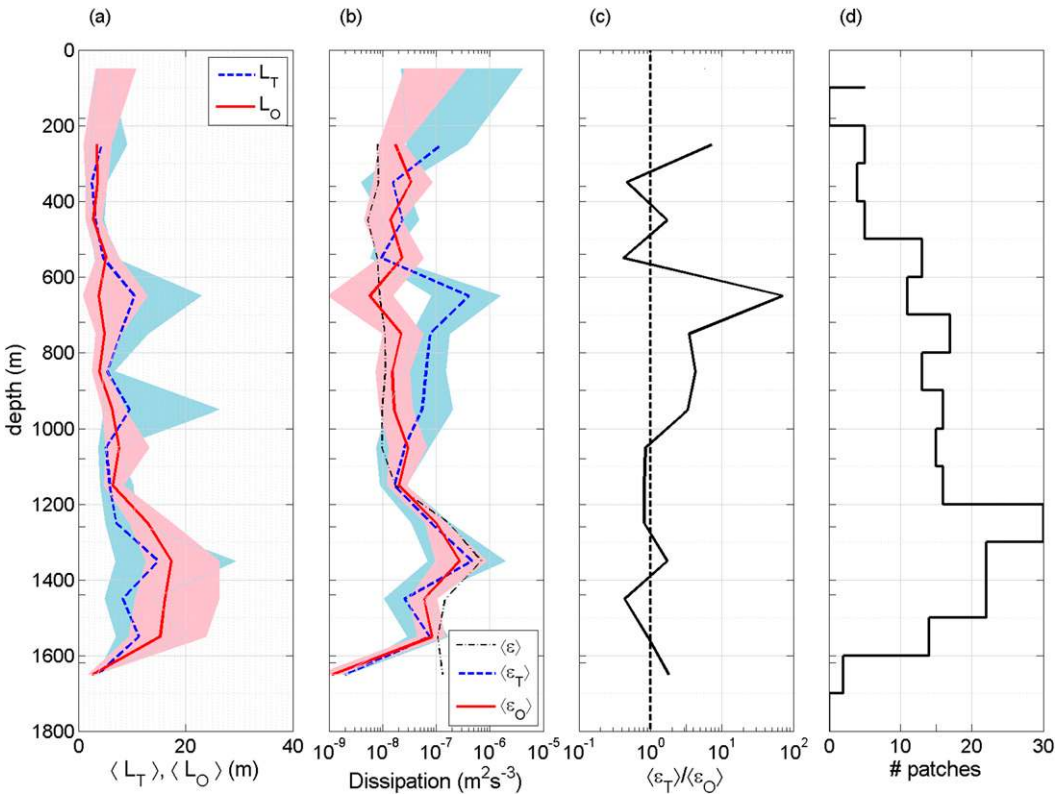

FIG. 11. Mean values as a function of depth at IWISE N2. The 95% confidence intervals around the means are shown in the left two panels.

the smaller overturns being representative of older turbulence. The intermediately sized overturn centered at 800 m is exemplary of middle-aged turbulence where $L_T \approx L_O$, while the smallest overturn near 850 m is exemplary of the old, well-mixed turbulence occupying regime C. Specific patchwise parameter values are included in the figure's caption.

Regime B is populated with the weakly forced, small overturns of NATRE and BBTRE data that are occurring in the presence of stronger stratification. This regime is perhaps analogous to the buoyancy-dominated regime of Mater and Venayagamoorthy (2014), where assumption 1 may hold but assumption 2 is likely violated because of buoyancy-induced anisotropy at the outer scales that effectively truncates the inertial subrange to smaller scales. Taken together, however, weakly forced data of regimes B and C indicate a central tendency of $L_T \approx L_O$ in agreement with classic thermocline observations.

It is important to reiterate that the regime labels in Fig. 6 are not meant to quantitatively delineate the regimes. Their placement is loosely based on the range of scales expressed by the current datasets. The K–H turbulence within the thermocline—in part convectively driven—would also be expected to evolve between these regimes, likely from A to B or C, but over a smaller range of scales than that suggested by the label placement in Fig. 6. At the resolution of Fig. 6, the signature of small-scale K–H events is likely obscured by other marginally stable shear-driven processes (e.g., turbulence driven by uniform shear).

A summary of the mean trends in L_T/L_O as a function of $\widehat{L_T}$ for all three datasets is shown in Fig. 9. The mean N for each bin in $\widehat{L_T}$ is expressed in the marker colors. Interestingly, the BBTRE data demonstrate a slightly lower slope and a higher intercept than the IWISE data and seem to bridge the gap between the NATRE data in the limit of low $\widehat{L_T}$ and the IWISE data at high $\widehat{L_T}$. This difference is perhaps attributable to the presence of multiple turbulent processes in BBTRE; the region shares characteristics of NATRE (weak thermocline turbulence) and those of IWISE (hydraulic/convective instabilities) as well as having boundary shear on canyon slopes. The relative abundance of boundary shear-driven turbulence and weaker thermocline turbulence in BBTRE, both of which are associated with smaller $\widehat{L_T}$ values and $L_T/L_O \approx 1$, is likely responsible for the decreased slope and increased intercept. Furthermore, BBTRE demonstrates relatively weak and consistent

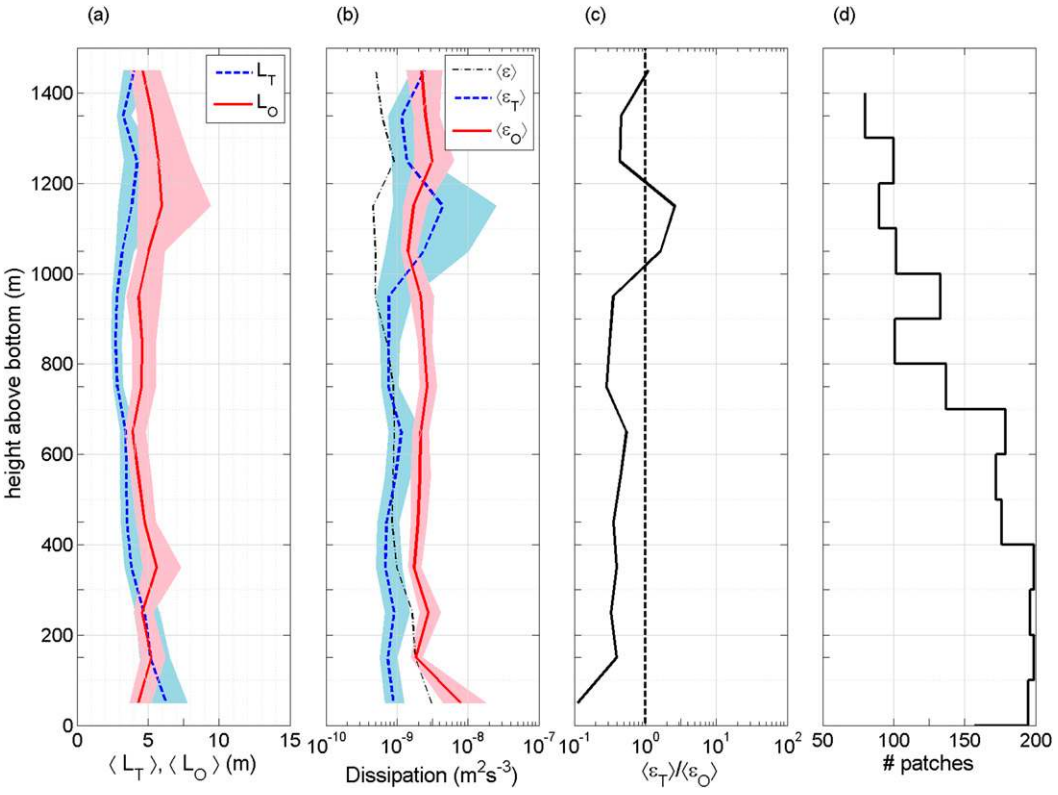

FIG. 12. Mean values as a function of height above bottom for BBTRE. The 95% confidence intervals around the means are shown in the left two panels.

stratification for all $\widehat{L_T}$ when compared to IWISE. In IWISE, stratification decreases with decreasing $\widehat{L_T}$ as might be expected of convective instabilities that mix the fluid. The lack of a clear correlation between N and $\widehat{L_T}$ in BBTRE supports the notion that turbulence is generated by multiple mechanisms in addition to the hydraulic/convective type.

The results above suggest that while $\widehat{L_T}$ is perhaps indicative of the turbulence age for a given set of observations, the parameter does not necessarily allow for a straightforward comparison between flows where turbulent processes differ. A comprehensive generalization of L_T/L_O is likely not possible given that real flows depend on various quantities in addition to those typically available (e.g., L_T, N, ν). Nonetheless, the monotonic increase in L_T/L_O with increasing $\widehat{L_T}$ is statistically significant and suggests a possibility for the overestimation of the dissipation rate via Eq. (1) when sampling favors overturns that exceed some mechanism-specific threshold in $\widehat{L_T}$. For the convectively driven turbulence of IWISE, that threshold appears to be $\widehat{L_T} \approx 175$.

b. *Mean profiles*

Comparisons of the previous section indicate that there is a central tendency for $L_T/L_O \approx 1$ when all datasets are considered despite an obvious dependence on the nondimensional Thorpe scale $\widehat{L_T}$. Does this dependence result in a bias when sample size is reduced in regions where convectively driven turbulence is thought to dominate? To address this question we consider the Thorpe–Ozmidov relationship as a function of depth, where sample sizes are restricted to discrete depth horizons in a fashion similar to Ferron et al. (1998) or Alford et al. (2011). Mean profiles of dissipation are desirable because they allow for vertical descriptions of turbulent mixing that are important in large-scale ocean circulation models (Melet et al. 2013).

For all datasets, patchwise length scales, buoyancy frequency, and dissipation rates were averaged in 100-m vertical bins across profile ensembles. These ensemble-averaged values are denoted with angled brackets $\langle\,\rangle$ and are shown as a function of depth in Figs. 10–14 for IWISE L profiles taken during the spring tidal period (34 profiles), IWISE N2 (all 10 profiles, also taken during the spring tidal period), near-bottom BBTRE, upper-ocean NATRE, and deep-ocean NATRE, respectively. Because topographic relief at the BBTRE site varies from station to station by $O(10^3)$ m, average values from BBTRE are shown as a function of distance above the local bottom (Fig. 12).

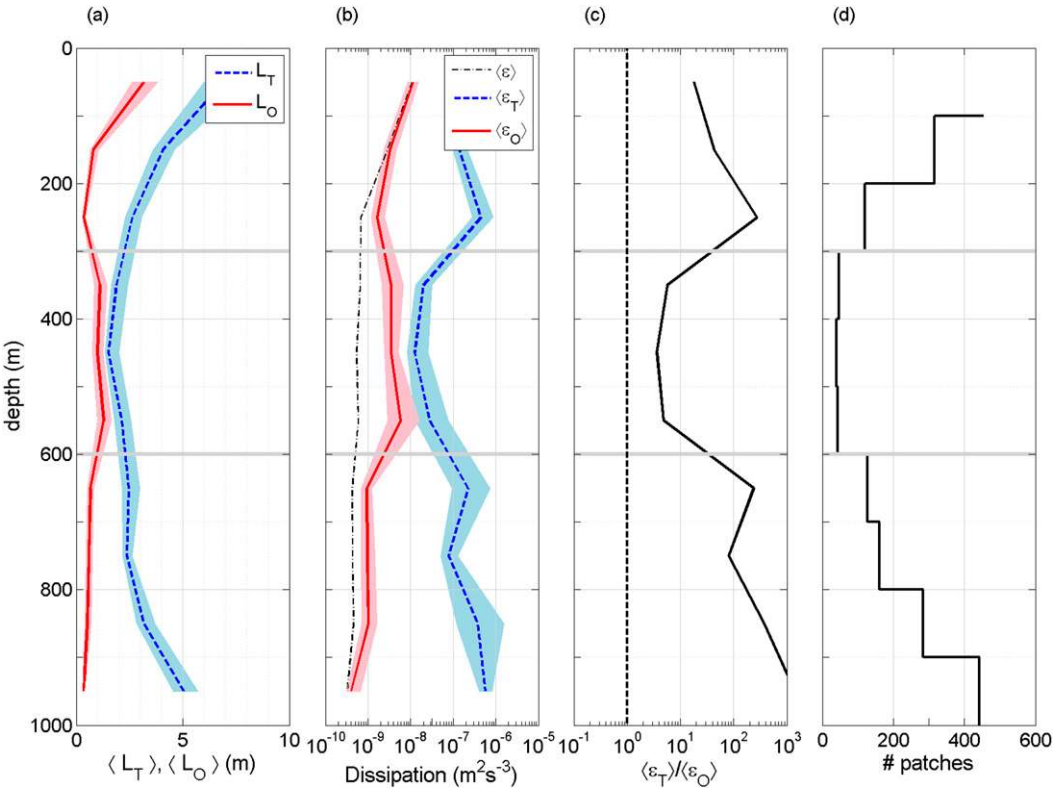

FIG. 13. Mean values as a function of depth upper-ocean depths of NATRE. The 95% confidence intervals around the means are shown in the left two panels. Only data from 300 to 600 m (bracketed by heavy gray lines) are used in analysis.

In qualitative agreement with Ferron et al. (1998), the average inferred dissipation rate $\langle \epsilon_T \rangle$ is generally greater than, but within an order of magnitude of, the average measured dissipation rate within the overturns $\langle \epsilon_O \rangle$. First, consider the IWISE stations where large overturns drive convective turbulence. Profiles from the L site (see Fig. 10) indicate a subtle bias toward $\langle \epsilon_T \rangle > \langle \epsilon_O \rangle$ that is marginally significant throughout the water column according to bootstrapped 95% confidence intervals around the means. Profiles for the N2 site (see Fig. 11) show a similar bias from about 600 to 1000 m but excellent agreement below 1200 m. Given the relatively quiet microstructure signal in the thermocline of N2, it is possible that the bias there is influenced by salinity-compensated temperature inversions. Considering only the near-bottom N2 data, the difference between the excellent agreement at N2 and the high bias at L may be due to a relatively strong contribution of bottom-enhanced shear at N2. Additional boundary layer shear would act to increase the number of small overturns and mitigate any potential bias induced by large convective instabilities. Interestingly, the high bias at IWISE L exists despite the fact that the 34 profiles collectively average over roughly six diurnal cycles of the tide. This indicates that the bias is physically based and suggests a dependence on the convectively driven turbulence that characterizes the site. It is important to note, however, that nonlocal dissipation due to tidal advection (a sampling-based bias) cannot be ruled out conclusively and could also drive the high bias at IWISE L if the profiles disproportionately favor young turbulence.

Next, consider the BBTRE site where topographic roughness promotes bottom-enhanced turbulence driven by a range of processes that likely include upward-propagating internal waves, shear due to bottom drag, and larger-scale processes that lead to convective instability such as the lee waves and hydraulic jumps suggested by Thurnherr et al. (2005). Measured dissipation (see dashed–dotted line in Fig. 12b) and the number of overturns (Fig. 12d) increase with depth as a result of these processes. Interestingly, and in contrast with IWISE, the processes of BBTRE result in a bias toward $\langle \epsilon_T \rangle < \langle \epsilon_O \rangle$ over the bottommost 1000 m (Fig. 12b). This low bias is directly attributable to the relatively high concentration of data in regime C of Fig. 6 in which $L_T < L_O$. Recall that regime C is characterized by small overturns in weak stratification and may

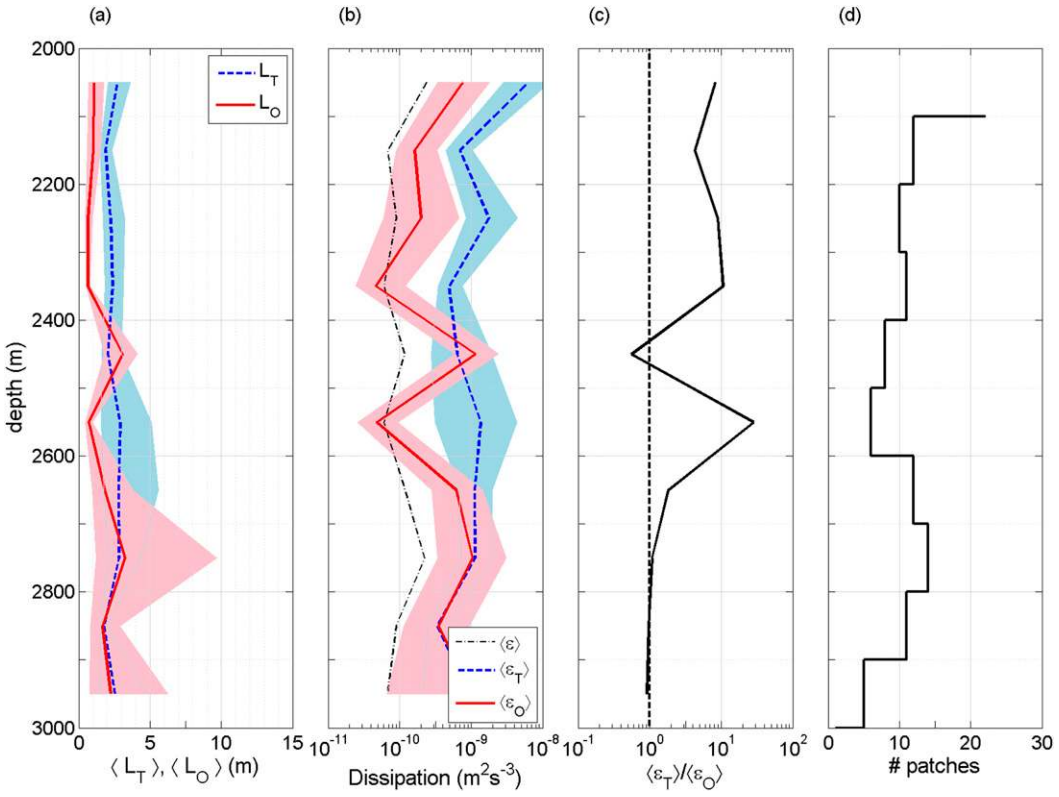

FIG. 14. Mean values as a function of depth for deep-ocean depths of NATRE. The 95% confidence intervals around the means are shown in the left two panels.

represent shear-dominated or late-stage convectively generated turbulence. A possible physical explanation for the bias is that boundary-related shear and smaller-scale processes are important in the near-bottom waters of BBTRE and/or that large overturns caused by hydraulic processes quickly lose coherency in the weak stratification so that they are less frequently observed. The relatively weak stratification of BBTRE also gives rise to a potential technical source of bias in the choice of instrument noise level for filtering the potential temperature signal. As discussed in Gargett and Garner (2008), we find that increasing the level of assumed instrument noise preferentially filters out small overturns; increasing the noise level above that used here would, therefore, effectively reduce the low bias.

Finally, consider the mean profiles from NATRE for the upper and deep ocean in Figs. 13 and 14, respectively. The depth range considered in our analysis for the upper ocean (300–600 m; bracketed by gray lines in Fig. 13) shows a marginally significant bias toward $\langle \epsilon_T \rangle > \langle \epsilon_O \rangle$ that is potentially influenced by salinity compensation. Outside this range, the influence of salinity compensation is stronger and the bias is much more pronounced. Data from the deep ocean indicate better agreement; however, the relative scarcity of overturns inhibits a great deal of physical interpretation of the NATRE profiles. Compared to IWISE and BBTRE, the number of overturns seen in this dataset is relatively low for the relatively large number of profiles taken. As such, the average of the dissipation measured within overturns $\langle \epsilon_O \rangle$ (red lines in Figs. 13b and 14b) is significantly higher than the average of the total measured dissipation $\langle \epsilon \rangle$ (dashed–dotted lines) for most depths; the quiescent background flow is significantly less energetic than the few infrequent overturns. We mention in passing that this condition presents an additional concern in praxis if Eq. (1) is to be used to infer ambient dissipation levels in relatively quiet flows.

c. *Time integration: Energy budgets*

Of particular importance to ocean circulation models is the correct budgeting of kinetic energy between various sources and sinks so that models are energetically consistent. The two important sinks are, of course, viscous dissipation and conversion to mean potential energy via diapycnal buoyancy flux. Commonly, the latter is related to the former using a prescribed mixing efficiency via the Osborn parameterization (Osborn 1980).

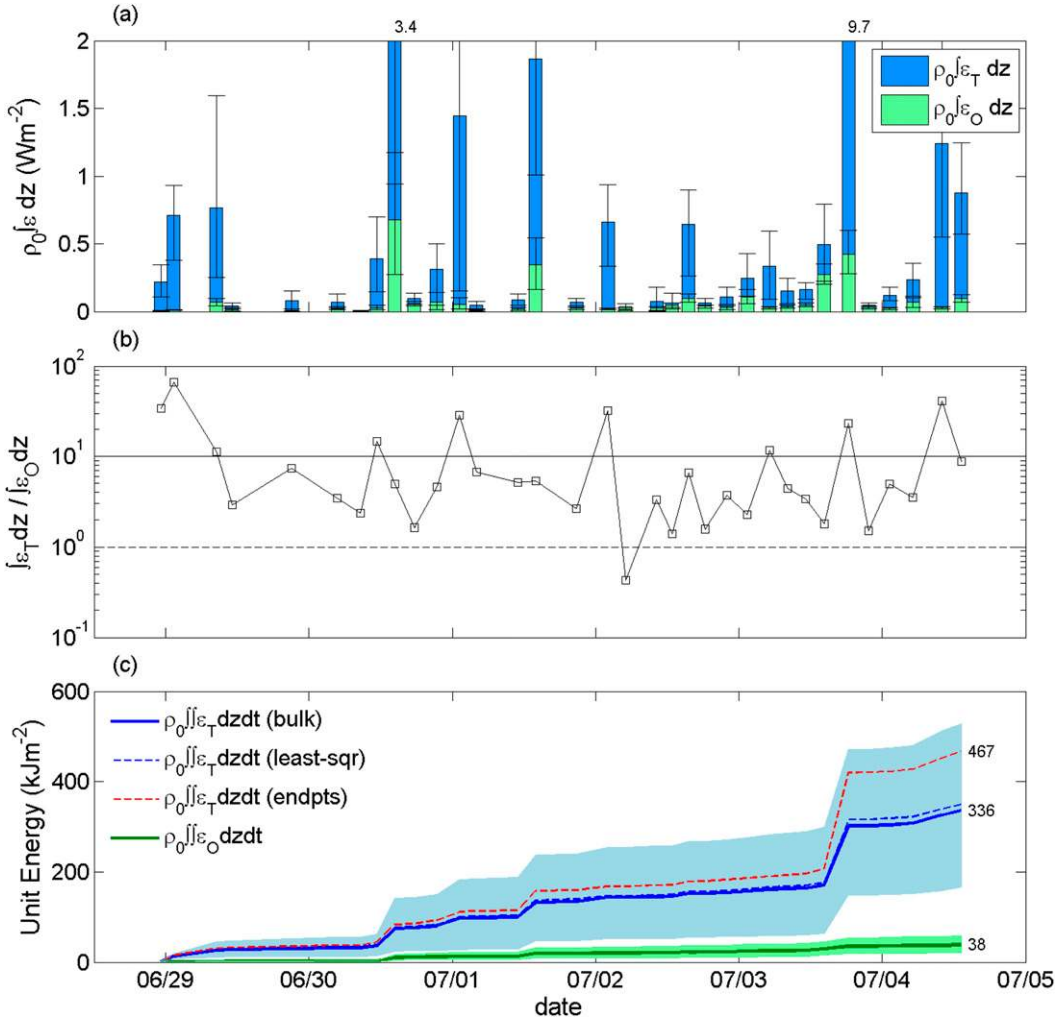

FIG. 15. (a) Unit power from depth integration of measured and Thorpe scale–inferred dissipation rates, (b) ratio of inferred to measured unit power, and (c) unit energy dissipated determined by time integration of unit powers for profiles taken at IWISE L over a spring tidal period. Bootstrapped 95% confidence intervals in (a) were developed based on the assumption that the patchwise dissipation rates captured by a given profile represent a subsample of a larger population. The confidence bands around the inferred (for bulk gradient method) and measured energy curves in (c) were developed from the confidence intervals in (a) and the cases of either consistent over or underestimation. Alternative methods for calculating N are compared in the bottom panel. The value $a = 1$ is used in all calculations of ϵ_T.

As such, time integration of ϵ in turbulent regions of the ocean provides a means for estimating the total energy consumed by the turbulence during a given period of time. Therefore, time-integrated values (rather than the mean profiles discussed above) provide valuable information for the calibration and validation of numerical models. In this section, we consider the possibility of using ϵ_T for this purpose and thereby indirectly evaluate the effectiveness of time integration in smoothing over the phase difference between APE of the large overturns and TKE of the subsequent turbulence. Moreover, the analysis is a preliminary test on the validity of applying Eq. (1) to instantaneous realizations of the density field. Data from IWISE L sites during the spring tidal period are considered because of the quasi-continuous nature of the profiles and their close proximity to one another.

Integration of measured dissipation values with respect to depth for each profile gives a time series of the power lost to viscous dissipation per unit surface area. Time integration then gives the monotonic record of unit energy dissipated. With the assumption of constant density ρ_0, the vertically time-integrated dissipation (i.e., unit energy) is estimated from VMP measurements using

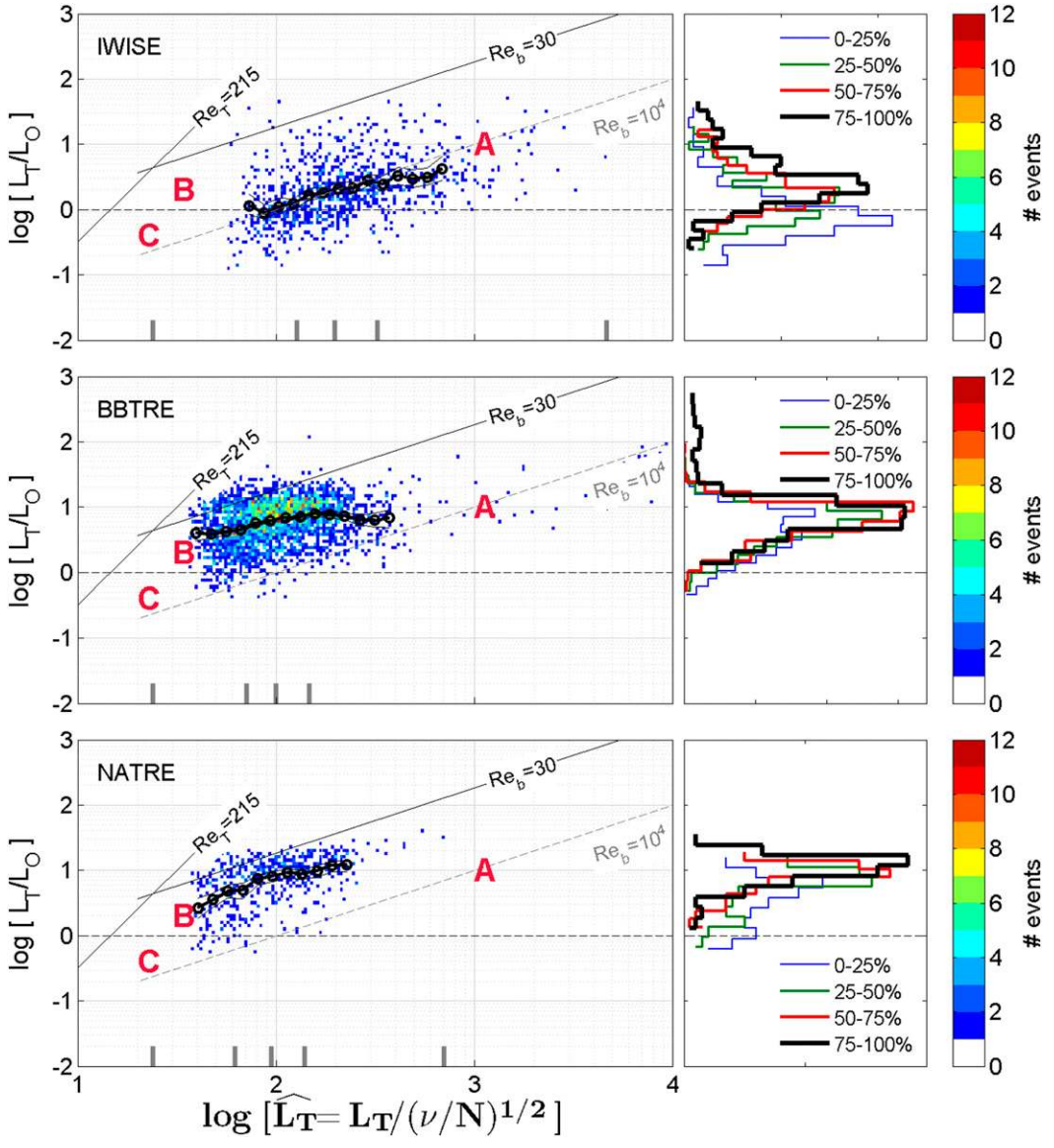

FIG. A1. Analysis rerun using density sorting for comparison with temperature-sorted values of Fig. 6. (top) IWISE, (middle) BBTRE, and (bottom) NATRE. Shown for assumed noise levels of 0.001 kg m^{-3} for IWISE and 0.0005 kg m^{-3} for BBTRE and NATRE.

$$\text{Unit Energy(patches)} \approx \rho_0 \sum_{i=1}^{n} \sum_{j=1}^{m} (\epsilon_O \Delta z_{\text{patch}})_{j,i} \Delta t_i, \quad (8)$$

where n is the total number of profiles ($n = 34$ at IWISE L during the spring tidal period), m is the total number of patches with $L_T > 1$ m in a given profile, $\Delta z_{\text{patch},j}$ is the vertical extent of a given patch, and Δt_i is the central differenced time increment allotted to each profile ($\Delta t \approx 4$ hr at IWISE L). Analogously, Thorpe scale–inferred unit energy is estimated using

$$\text{Unit Energy(Thorpe)} \approx \rho_0 \sum_{i=1}^{n} \sum_{j=1}^{m} (\epsilon_T \Delta z_{\text{patch}})_{j,i} \Delta t_i. \quad (9)$$

Depth- and time-integrated values of ϵ_O and ϵ_T are shown in Fig. 15. Measured unit power (shown as green bars in Fig. 15a) demonstrates high temporal variability and is extremely high by open-ocean standards with some values approaching or exceeding 0.5 W m^{-2}. While roughly in phase with measured values, the Thorpe scale–inferred unit power (shown as blue bars) exceeds direct measurements by over an order of magnitude for several of the profiles and is greater than the measured power for all but one profile (Fig. 15b). Bootstrapped 95% confidence intervals around the depth-integrated value in Fig. 15a were developed based on the assumption that the patchwise dissipation rates captured by a

given profile represent a subsample of a larger population occurring in the vicinity of the VMP cast (note that depth-integrated dissipation is simply the patch thickness–weighted mean for a given profile multiplied by the sum of patch thicknesses; therefore, bootstrapping can be done on the weighted mean and confidence intervals transferred to the depth-integrated value). The confidence intervals then represent the variability expected if several simultaneous VMP casts had been made.

The dramatic overestimation occurs partly because of the lognormal nature of L_T/L_O that allows for rare but large overturns (for which $\epsilon_T \gg \epsilon_O$) to heavily weight estimates of power for an individual profile. In other words, the bias in the Thorpe scale–based method can be very large on a patchwise basis for large events from the right tail of the distribution of L_T/L_O (i.e., from regime A of Fig. 6). Such an overturn was recorded in the profile taken at 1820 UTC on 3 July and is responsible for a large jump in the time series of inferred dissipation (blue line in Fig. 15c). The bias is further magnified as a result of effectively weighting ϵ_T by patch size; since Δz_{patch} correlates with L_T (not shown), the bias toward $\epsilon_T > \epsilon_O$ that occurs at large L_T is magnified in the estimates of power from $\sum_{j=1}^{m}(\epsilon_T \Delta z_{\text{patch}})_j$.

Consistent overestimation of unit power by the Thorpe scale–based method results in a time-increasing overestimation of the dissipated energy shown in Fig. 15c. Over the course of the spring tidal period, the energy inferred to have dissipated (336 kJ m^{-2} using the bulk method for N) is nearly 9 times greater than that which was directly measured within turbulent patches (38 kJ m^{-2}) and nearly 6 times greater than that which was measured over the total depth (57 kJ m^{-2}; not plotted). The confidence bands around the inferred and measured energy curves in Fig. 15c were developed from the bootstrapped 95% confidence intervals in Fig. 15a and the cases of either consistent overestimation or underestimation.

As in the preceding analyses, all calculations of ϵ_T use $a = 1$ in Eq. (1). To examine the sensitivity to a, the inferred time-integrated dissipation was calculated using the value found by Dillon (1982), $a = 0.8$, and the value suggested by the geometric mean of the data $a = 1.09$ listed in Table 1 (results not plotted). The lower value still gives an inferred dissipation (215 kJ m^{-2}) that is roughly 4 times greater than the total depth direct estimate, while the higher value results in a sevenfold overestimation (399 kJ m^{-2}).

Inferred values of time-integrated dissipation were also calculated using the alternative estimates of N discussed in section 4c. The sensitivity is shown in the Fig. 15c. Both alternative methods of obtaining N magnify the bias because they generally predict higher patchwise density gradients [i.e., higher values of N used in Eq. (1)]. Sudden amplification of the bias by the endpoint method near the end of the time series (large jump in the dashed red line in Fig. 15c just before 4 July) is due to a single large turbulent patch (mentioned above) that extended below the maximum depth of the profile so that the deep end point of the sorted temperature profile is not accurately represented for that patch. Prior to this anomaly, the methods are reasonably close to one another, with the endpoint and least squares methods being approximately 20% and 3% larger than the bulk method, respectively.

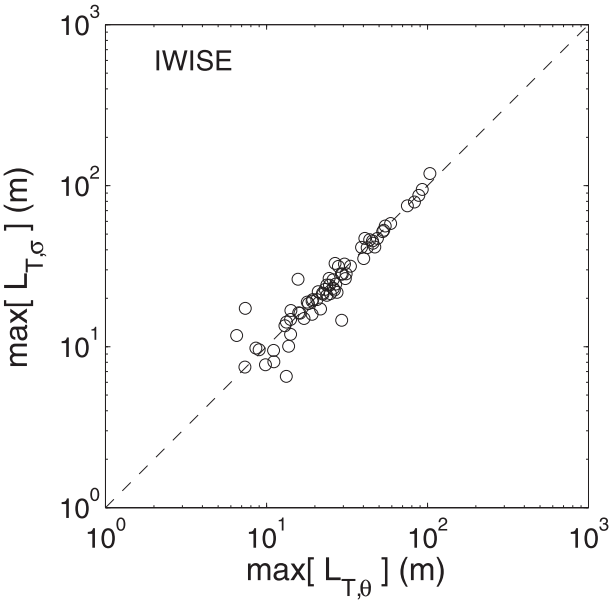

FIG. A2. Comparison of largest temperature-sorted overturn with largest density-sorted overturn on a profile-by-profile basis for IWISE VMP data. Shown for assumed noise levels of 0.001°C and 0.001 kg m^{-3}.

Results of the time integration indicate that large overestimation by the Thorpe scale–based method seen in some profiles is not balanced by underestimation in others. A possible physical explanation for the high bias is that temporal integration smooths over the lag between APE and TKE (i.e., assumption 1 is satisfied), but assumption 2 remains invalid in the mean. That is, while L_T quite possibly indicates the TKE present in the flow on average—as suggested by the results of Moum (1996) and Mater and Venayagamoorthy (2014)—it remains unclear whether it is also representative of the dissipation of TKE, even in a time-integrated sense. As discussed in section 5b regarding the bias in Fig. 10b, lateral advection leading to nonlocal dissipation may also be contributing to the bias seen here.

6. Conclusions

Using datasets from three different oceanic settings, we have shown that L_T increases with respect to L_O as a

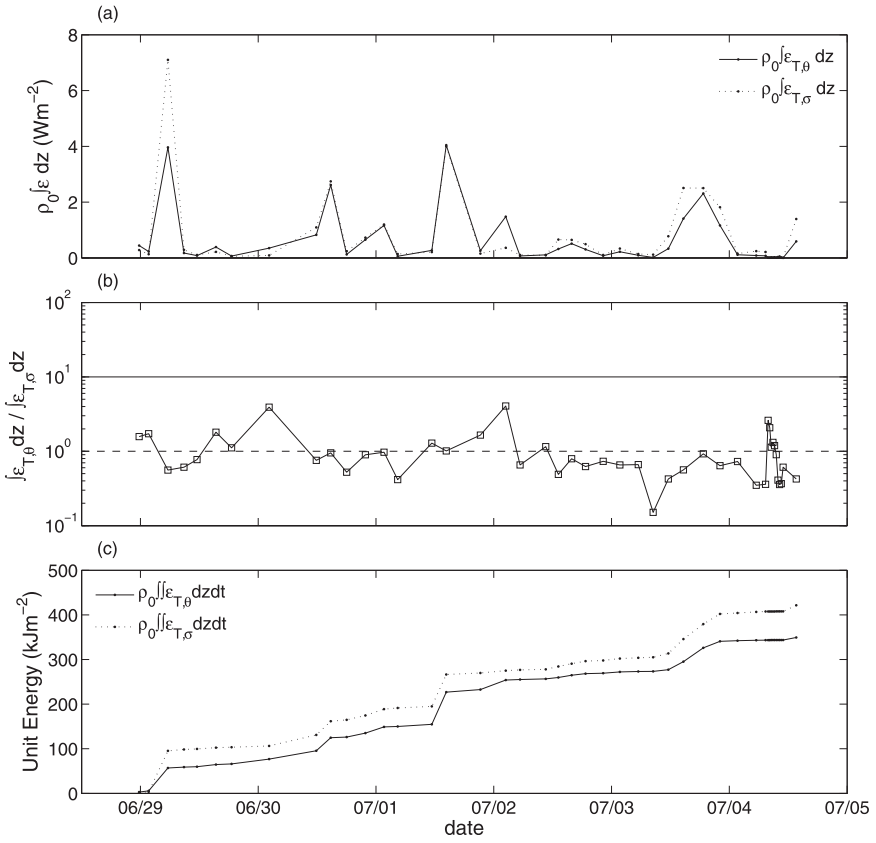

FIG. A3. Comparison of Thorpe scale–inferred dissipation using temperature sorting $\epsilon_{T,\theta}$ and density sorting $\epsilon_{T,\sigma}$ of CTD data for the locations and time period of Fig. 15. Unit power from (top) depth integration, (middle) ratio of temperature-sorted to density-sorted unit power, and (bottom) unit energy dissipated determined by time integration of unit powers. The value $a = 1$ is used in all calculations of ϵ_T and a noise level of 0.001 kg m^{-3} is assumed.

function of overturn size in a fashion analogous to Kelvin–Helmholtz turbulence. We suspect that this trend is a fundamental characteristic of convectively driven turbulence common to both K–H billows and the much larger-scale instabilities observed at the Luzon Strait and, to a lesser extent, the deep Brazil basin. The trend therefore presents a source of positive bias in Thorpe scale–inferred dissipation rates when sampling favors the largest overturns of such flows. Perhaps more concerning is that the ability of averaging techniques to smooth over this trend has thus far received minimal attention for these kinds of flows.

To assess the potential for bias, the current work has compared the Thorpe and Ozmidov scales as well as inferred and direct estimates of dissipation in various ways reflecting the various applications of the Thorpe scale–based method. In support of the earliest works that focused on all-inclusive ensembles, bias is not apparent when all samples are geometrically averaged irrespective of overturn size or depth. These bulk averages indicate the geometric mean of L_T/L_O is close to unity. A clear exception may be in the weakly turbulent flows of NATRE where double-diffusive structure can be misinterpreted as overturns—an additional condition leading to positive bias in Thorpe scale–inferred dissipation.

The agreement suggested by bulk geometric averaging generally transfers to depthwise averages of inferred and directly measured dissipation rate, although, the mean profiles at IWISE L suggest a marginally significant positive bias in Thorpe scale–inferred dissipation that is likely related to the large convective instabilities occurring there. The bias exists despite representation of all phases of the tidal cycle—a finding that suggests the physical conditions supporting $L_T \sim L_O$ are not met in convectively generated turbulence even when both young and old turbulence are represented in the observations. Alternatively, the IWISE L profiles may have been collected close to the generation site of the instabilities and, thus, disproportionately favored young turbulence, regardless of tidal phase. Unfortunately, neither the violation of physical conditions nor sampling

error can be verified with the current measurements. The billow-tracking observations of Seim and Gregg (1994) support the latter explanation in the context of K–H instabilities, albeit with "wide scatter" and fewer observed overturns than reported here. Additional campaigns tracking billows like those generated at IWISE L are needed to separate sampling biases from physically based biases that may exist. Such campaigns should also consider the influence that boundary length scales have on the scaling—an important physical bias in topographically influenced overturning not explicitly investigated here (see, e.g., Chalamalla and Sarkar 2015).

Interestingly, and despite fewer profiles, the bias is not as apparent at the IWISE N2 site that shows excellent agreement in the lower 500 m—a finding we suggest may be related to strong bottom shear and local dissipation. In the case of BBTRE, the trend in L_T/L_O as a function of overturn size is less pronounced than in IWISE, and, accordingly, the positive bias does not appear in the mean profiles. Instead, inferred dissipation is biased low because of a large number of small overturns in the relatively weak stratification. We have proposed that the abundance of small overturns is due to an array of smaller-scale, boundary-related processes that may be overwhelming any bias because of short-lived convective instabilities.

The overestimation of dissipation by the Thorpe scale–based method seen in the mean profiles at IWISE L is especially apparent upon time integration. Such an application of the method is potentially dangerous because of the emphasis placed on instantaneous realizations of the temperature (density) field rather than statistical averages and may lead to field-based inferences and numerical models that are too dissipative and diffusive; the positive bias in the integration method is exacerbated by the presence of rare, large events with $L_T/L_O \gg 1$.

While it may be tempting to employ Eq. (1) when overturns are an obvious feature of the turbulence, the results shown here suggest that patchwise use of the method is significantly biased by the state and/or age of the observed overturns. Hence, incomplete sampling (a particularly vexing problem encountered when observing naturally occurring geophysical flows) will lead to biases in dissipation estimates from Thorpe scales. Therefore, use of Eq. (1) in regions characterized by large overturns that convectively drive the turbulence should be approached with caution, especially when overturns span a large range in scales, sample sizes are small, or when individual events are integrated. Furthermore, the appropriate question regarding the Thorpe–Ozmidov relation when dealing with convectively generated turbulence may not be "how many samples are needed?" but rather "are the physical conditions appropriate?" This question is addressed by a companion paper in the context of direct numerical simulations (see Scotti 2015).

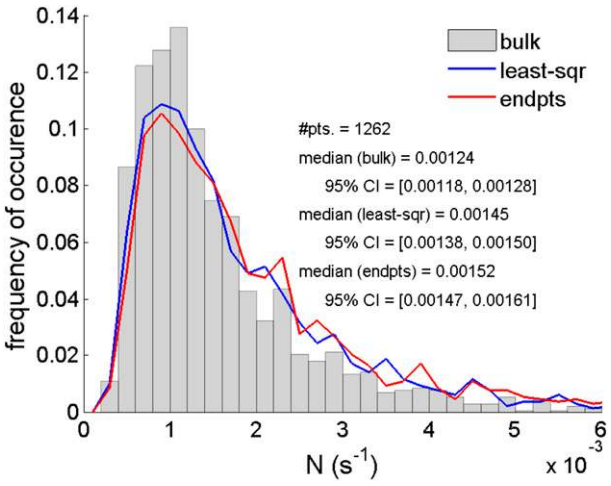

FIG. B1. Comparisons of N values for different methods of calculating the patchwise density gradient $\partial\bar{\sigma}/\partial z$ for patches identified in IWISE.

Acknowledgments. B.D.M. and S.K.V. gratefully acknowledge the support of the Office of Naval Research under Grants N00014-12-1-0279, N00014-12-1-0282, and N00014-12-1-0938 (Program Manager: Dr. Terri Paluszkiewicz). S.K.V. also acknowledges support of the National Science Foundation under Grant OCE-1151838. L.S.L. acknowledges support for BBTRE by the National Science Foundation by Contract OCE94-15589 and NATRE and IWISE by the Office of Naval Research by Contracts N00014-92-1323 and N00014-10-10315. J.N.M. was supported through Grant 1256620 from the National Science Foundation and the Office of Naval Research (IWISE Project). The authors also wish to thank A. Scotti for discussions on the subject and the three anonymous reviewers for their constructive criticisms.

APPENDIX A

Temperature versus Density Sorting

Our analysis uses potential temperature as a surrogate for potential density in the Thorpe-scale calculations out of concerns over the noise and reliability of salinity measurements. To check on the sensitivity of our analysis to salinity-compensated temperature inversions, the analysis was rerun for all datasets using potential density (with indirectly estimated salinity for the IWISE data; see below) and plotted here in Fig. A1. The data

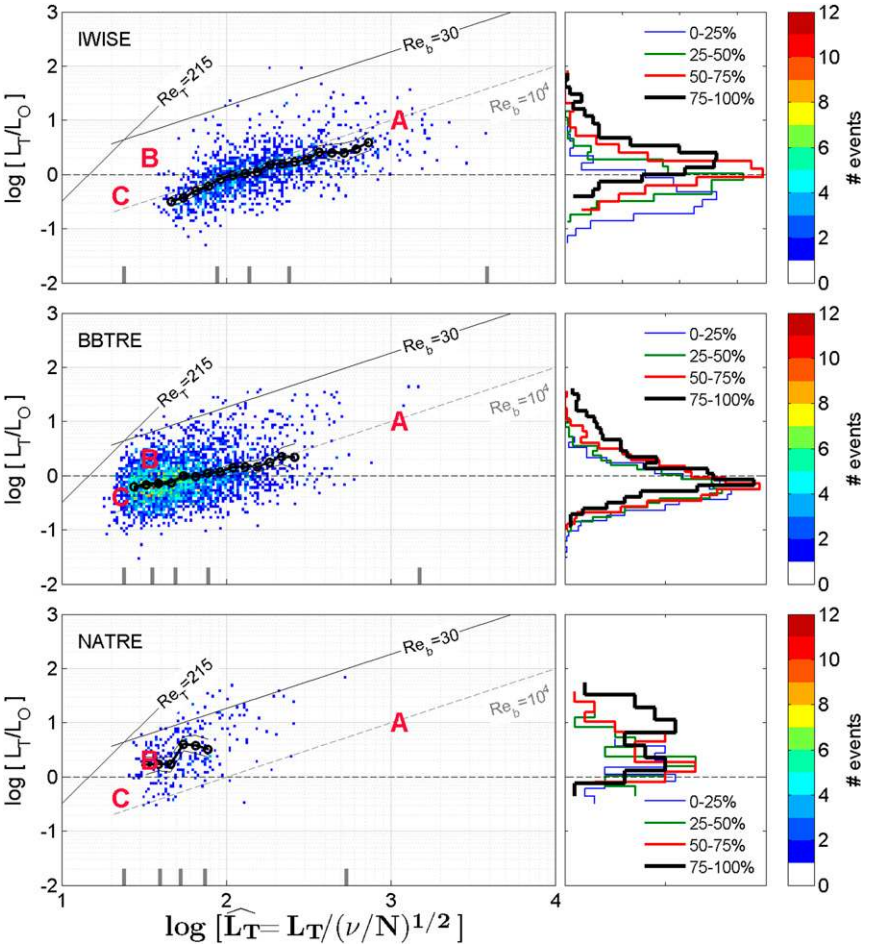

FIG. B2. Analysis rerun using the least squares gradient for calculation of N. (top) IWISE, (middle) BBTRE, and (bottom) NATRE. Compare with Fig. 6.

generally shift to higher values of L_T/L_O—most likely due to added salinity noise. However, the general trend of increasing L_T/L_O with increasing $\widehat{L_T}$ remains. As such, the discussion of section 5a regarding this trend remains pertinent.

Two additional tests were performed on the IWISE data that have been most prominently featured in this work. To circumvent problematic issues with VMP conductivity measurements, the first of these tests uses indirect salinity values derived from temperature measurements of the VMP and a fit to the T–S relationship provided by nearby and quasi-simultaneous CTD casts. The largest temperature-sorted Thorpe-scale value $L_{T,\theta}$ is then compared to the largest density-sorted value $L_{T,\sigma}$ on a profile-by-profile basis in Fig. A2 for all casts of the VMP. The correlation is quite good and does not discourage the use of potential temperature as a surrogate for density.

The second, and perhaps more convincing, test focuses solely on the CTD measurements and thus avoids problems associated with indirectly estimating salinity. Inferred values of dissipation using temperature and density sorting are shown in Fig. A3 for the locations and time period corresponding to the VMP measurements of Fig. 15. The two methods give consistent results for all but the third cast in which a single density inversion biases $\epsilon_{T,\sigma}$ high. It is also worth noting that the inferred energy consumed ($\approx$400 kJ m^{-2}) is in close agreement with the inferred value based on VMP measurements (Fig. 15c).

APPENDIX B

Comparison of N Estimates

We use the method of Smyth et al. (2001) to calculate N because it gives a bulk density gradient that is relatively insensitive to patch boundaries. In Fig. B1, estimates of N determined from the bulk method are compared to those obtained from an average gradient

that uses the highest and lowest $\tilde{\sigma}$ values for a given patch (i.e., end points of the Thorpe-sorted $\tilde{\sigma}$ within a patch) for patches identified in IWISE. A third method, wherein the gradient is determined from a least squares fit to Thorpe-sorted $\tilde{\sigma}$, is also compared. The distributions indicate that the bulk method predicts slightly lower values of N than the other methods. Indeed, bootstrapped 95% confidence intervals around the medians of the distributions indicate that the bulk method is significantly different than the other two methods that are statistically the same (i.e., the confidence interval around the bulk median does not overlap with those of the other methods). This holds true for BBTRE and NATRE as well (not shown). To evaluate the impact of the choice of method, the analysis was rerun using the least squares method. The results are shown here in Fig. B2. Despite the statistical difference in N values, a visual comparison of Fig. B2 with Fig. 6 does not reveal concerning differences. To more quantitatively examine the sensitivity of the analysis to choice of N, the time integration of section 5c was rerun using all three methods. The results were discussed in section 5c and shown in Fig. 15c.

REFERENCES

Alford, M. H., and Coauthors, 2011: Energy flux and dissipation in Luzon Strait: Two tales of two ridges. *J. Phys. Oceanogr.*, **41**, 2211–2222, doi:10.1175/JPO-D-11-073.1.

Buijsman, M. C., and Coauthors, 2014: Three-dimensional double-ridge internal tide resonance in Luzon Strait. *J. Phys. Oceanogr.*, **44**, 850–869, doi:10.1175/JPO-D-13-024.1.

Chalamalla, V. K., and S. Sarkar, 2015: Mixing, dissipation rate, and their overturn-based estimates in a near-bottom turbulent flow driven by internal tides. *J. Phys. Oceanogr.*, **45**, 1969–1987, doi:10.1175/JPO-D-14-0057.1.

Crawford, W. R., 1986: A comparison of length scales and decay times of turbulence in stably stratified flows. *J. Phys. Oceanogr.*, **16**, 1847–1854, doi:10.1175/1520-0485(1986)016<1847:ACOLSA>2.0.CO;2.

Dillon, T. M., 1982: Vertical overturns: A comparison of Thorpe and Ozmidov length scales. *J. Geophys. Res.*, **87**, 9601–9613, doi:10.1029/JC087iC12p09601.

Dougherty, J. P., 1961: The anisotropy of turbulence at the meteor level. *J. Atmos. Terr. Phys.*, **21**, 210–213, doi:10.1016/0021-9169(61)90116-7.

Ferron, B., H. Mercier, K. Speer, A. Gargett, and K. Polzin, 1998: Mixing in the Romanche fracture zone. *J. Phys. Oceanogr.*, **28**, 1929–1945, doi:10.1175/1520-0485(1998)028<1929:MITRFZ>2.0.CO;2.

Gargett, A., and T. Garner, 2008: Determining Thorpe scales from ship-lowered CTD density profiles. *J. Atmos. Oceanic Technol.*, **25**, 1657–1670, doi:10.1175/2008JTECHO541.1.

Gibson, C. H., 1980: Fossil temperature, salinity, and vorticity turbulence in the ocean. *Marine Turbulence Proceedings of the 11th International Liège Colloquium on Ocean Hydrodynamics*, J. C. J. Nihoul, Ed., Elsevier Oceanography Series, Vol. 28, Elsevier, 221–257.

Gill, A. E., 1982: *Atmosphere–Ocean Dynamics*. Academic Press, 662 pp.

Gregg, M. C., 1987: Diapycnal mixing in the thermocline. *J. Geophys. Res.*, **92**, 5249–5286, doi:10.1029/JC092iC05p05249.

Klymak, J. M., and S. M. Legg, 2010: A simple mixing scheme for models that resolve breaking internal waves. *Ocean Modell.*, **33**, 224–234, doi:10.1016/j.ocemod.2010.02.005.

Ledwell, J. R., E. T. Montgomery, K. L. Polzin, L. C. St. Laurent, R. W. Schmitt, and J. M. Toole, 2000: Evidence for enhanced mixing over rough topography in the abyssal ocean. *Nature*, **403**, 179–182, doi:10.1038/35003164.

Luketina, D. A., and J. Imberger, 1989: Turbulence and entrainment in a buoyant surface plume. *J. Geophys. Res.*, **94**, 12 619–12 636, doi:10.1029/JC094iC09p12619.

Mater, B. D., and S. K. Venayagamoorthy, 2014: A unifying framework for parameterizing stably stratified shear-flow turbulence. *Phys. Fluids*, **26**, 036601, doi:10.1063/1.4868142.

——, S. M. Schaad, and S. K. Venayagamoorthy, 2013: Relevance of the Thorpe length scale in stably stratified turbulence. *Phys. Fluids*, **25**, 076604, doi:10.1063/1.4813809.

Melet, A., R. Hallberg, S. Legg, and K. Polzin, 2013: Sensitivity of the ocean state to the vertical distribution of internal-tide-driven mixing. *J. Phys. Oceanogr.*, **43**, 602–615, doi:10.1175/JPO-D-12-055.1.

Moum, J. N., 1996: Energy-containing scales of turbulence in the ocean thermocline. *J. Geophys. Res.*, **101**, 14 095–14 109, doi:10.1029/96JC00507.

Munk, W., 1981: Internal waves and small-scale processes. *Evolution of Physical Oceanography*, B. A. Warren and C. Wunsch, Eds., The MIT Press, 264–291.

Osborn, T. R., 1980: Estimates of the local rate of vertical diffusion from dissipation measurements. *J. Phys. Oceanogr.*, **10**, 83–89, doi:10.1175/1520-0485(1980)010<0083:EOTLRO>2.0.CO;2.

Ozmidov, R. V., 1965: On the turbulent exchange in a stably stratified ocean (English translation). *Izv. Acad. Sci. USSR Atmos. Oceanic Phys.*, **1**, 853–860.

Polzin, K., J. Toole, J. Ledwell, and R. Schmitt, 1997: Spatial variability of turbulent mixing in the abyssal ocean. *Science*, **276**, 93–96, doi:10.1126/science.276.5309.93.

Rohr, J. J., E. C. Itsweire, K. N. Helland, and C. W. Van Atta, 1988: Growth and decay of turbulence in a stably stratified shear flow. *J. Fluid Mech.*, **195**, 77–111, doi:10.1017/S0022112088002332.

Schmitt, R. W., 1994: Double diffusion in oceanography. *Annu. Rev. Fluid Mech.*, **26**, 255–285, doi:10.1146/annurev.fl.26.010194.001351.

——, 1999: Spice and the demon. *Science*, **283**, 498–499, doi:10.1126/science.283.5401.498.

Scotti, A., 2015: Biases in Thorpe-scale estimates of turbulence dissipation. Part II: Energetics arguments from turbulence simulations. *J. Phys. Oceanogr.*, **45**, 2522–2543, doi:10.1175/JPO-D-14-0092.1.

Seim, H. E., and M. C. Gregg, 1994: Detailed observations of a naturally occurring shear instability. *J. Geophys. Res.*, **99**, 10 049–10 073, doi:10.1029/94JC00168.

Simmons, H. L., M.-H. Chang, Y.-T. Chang, S.-Y. Chao, O. Fringer, C. R. Jackson, and D. S. Ko, 2011: Modeling and prediction of internal waves in the South China Sea. *Oceanography*, **24**, 88–99, doi:10.5670/oceanog.2011.97.

Smyth, W. D., and J. N. Moum, 2013: Marginal instability and deep cycle turbulence in the eastern equatorial Pacific Ocean. *Geophys. Res. Lett.*, **40**, 6181–6185, doi:10.1002/2013GL058403.

——, ——, and D. R. Caldwell, 2001: The efficiency of mixing in turbulent patches: Inferences from direct simulations and microstructure observations. *J. Phys. Oceanogr.*, **31**, 1969–1992, doi:10.1175/1520-0485(2001)031<1969:TEOMIT>2.0.CO;2.

Stansfield, K., C. Garrett, and R. Dewey, 2001: The probability distribution of the Thorpe displacement within overturns in Juan de Fuca Strait. *J. Phys. Oceanogr.*, **31**, 3421–3434, doi:10.1175/1520-0485(2001)031<3421:TPDOTT>2.0.CO;2.

St. Laurent, L. C., 2012: Internal wave generation processes at deep-sills in the Luzon Passage region of the South China Sea. U.S. Office of Naval Research Tech. Rep., 11 pp.

——, and R. W. Schmitt, 1999: The contribution of salt fingers to vertical mixing in the North Atlantic Tracer Release Experiment. *J. Phys. Oceanogr.*, **29**, 1404–1424, doi:10.1175/1520-0485(1999)029<1404:TCOSFT>2.0.CO;2.

——, J. M. Toole, and R. W. Schmitt, 2001: Buoyancy forcing by turbulence above rough topography in the abyssal Brazil basin. *J. Phys. Oceanogr.*, **31**, 3476–3495, doi:10.1175/1520-0485(2001)031<3476:BFBTAR>2.0.CO;2.

——, H. L. Simmons, T. Y. Tang, and Y. Wang, 2011: Turbulent properties of internal waves in the South China Sea. *Oceanography*, **24**, 78–87, doi:10.5670/oceanog.2011.96.

Taylor, G. I., 1935: Statistical theory of turbulence. *Proc. Roy. Soc. London*, **A151**, 421–444, doi:10.1098/rspa.1935.0158.

Thorpe, S. A., 1977: Turbulence and mixing in a Scottish loch. *Philos. Trans. Roy. Soc.*, **A286**, 125–181, doi:10.1098/rsta.1977.0112.

Thurnherr, A. M., L. St. Laurent, K. G. Speer, J. M. Toole, and J. R. Ledwell, 2005: Mixing associated with sills in a canyon on the midocean ridge flank. *J. Phys. Oceanogr.*, **35**, 1370–1381, doi:10.1175/JPO2773.1.

Toole, J. M., R. W. Schmitt, and K. L. Polzin, 1994: Estimates of diapycnal mixing in the abyssal ocean. *Science*, **264**, 1120–1123, doi:10.1126/science.264.5162.1120.

Wesson, J. C., and M. C. Gregg, 1994: Mixing at Camarinal sill in the Strait of Gibraltar. *J. Geophys. Res.*, **99**, 9847–9878, doi:10.1029/94JC00256.

Wijesekera, H. W., T. M. Dillon, and L. Padman, 1993: Some statistical and dynamical properties of turbulence in the oceanic pycnocline. *J. Geophys. Res.*, **98**, 22 665–22 679, doi:10.1029/93JC02352.

Winters, K. B., P. N. Lombard, J. J. Riley, and E. A. D'Asaro, 1995: Available potential energy and mixing in density-stratified fluids. *J. Fluid Mech.*, **289**, 115–128, doi:10.1017/S002211209500125X.